California Polytechnic State University
San Luis Obispo, California 93407

Evaluation of Dual Flow
Thrust Vector Nozzles with
Exhaust Stream Impingement

Semi-Annual Progress Report 6/92-12/92
NASA-Ames Grant Number NAG 2-778

Thomas W. Carpenter, Principal Investigator & Professor,
Mechanical Engineering

Sean Dobbins, Mechanical Engineering Graduate Student

Steven Vaccarezza, Mechanical Engineering Graduate student

Introduction

To supplement previous work performed by NASA, A cold-jet test facility has been established at the California Polytechnic State University, San Luis Obispo campus. The purpose of this facility is to continue the studies of cold flow multiaxis thrust vectoring conducted at the NASA Langley Research Center. A single nozzle test apparatus has been completed and is presently operational. Included in this report are the results of the single flow test envelope that was requested by NASA personnel to fulfill NASA-Ames Grant Number NAG 2-778. Details about the test apparatus are included in the Cal Poly Semi-Annual Progress report for NASA-AMES Grant Number NCC2-748.

Symbols

F   Measured thrust along body axis, positive in forward direction, lbf

F_i ideal isentropic gross thrust, lbf

$$w_p \left\{ \frac{R_j T_{t,j}}{g^2} \frac{2\gamma}{\gamma-1} \left[1 - \left(\frac{1}{NPR} \right)^{(\gamma-1/\gamma)} \right] \right\}^{1/2}$$

F_n measured normal force, lbf

F_r resultant gross thrust, lbf

$$\sqrt{F^2 + F_N^2 + F_S^2}$$

F_s measured side force, lbf

g   acceleration due to gravity (where $1g = 32.174$ ft/sec^2)

R_j gas constant, 1716 ft^2/sec^2-°R

$T_{t,j}$ jet total temperature, °R

w_i ideal weight flow rate, lbf/sec

w_p measured weight flow rate, lbf/sec

g   ratio of specific heats, 1.4

δ_A, δ_B δ_C geometric deflection angle of vanes at positions A, B, and C, respectively, deg

δ_P resultant pitch thrust vector angle, $\tan^{-1}\dfrac{F_N}{F}$, deg

δ_Y resultant yaw thrust vector angle, $\tan^{-1}\dfrac{F_s}{F}$, deg

Abbreviations:

A   vane position A, upper

A/B   afterburner

B   vane position B, outer

C   vane position C, lower

NPR   nozzle pressure ratio

Test Envelope

The test envelope consisted of four sets of data. Each data set consisted of a configuration of two vanes set at fixed positions and the third vane was moved through a series of positions (-10, 0 ,5 10,15, 20, and 25 Deg.). The schematics used to represent each data set are shown in Figure 2. In addition, each data set was tested at three different nozzle pressure ratios. These pressure ratios were NPR 3, 4, and 5. In the first data set, the lower vane was fixed at 10 deg., the outer vane was fixed at -10 deg., and the upper vane was varied. In the second data set, the lower vane was fixed at 15 deg., the outer vane was fixed at -10 deg., and the upper vane was varied. In the third data set the lower vane was set at 10 deg., the upper vane was set at -10 deg., and the outer vane was varied. In the fourth data set, the lower vane was set at 15 deg., the upper vane was set at -10 deg., and the outer vane was varied. The entire test envelope consisted of 84 runs.

Test Method

For the single flow nozzle, 11 input channels were required. These channels corresponded to the upstream orifice plate temperature and pressure, the pressure drop across the orifice plate, the plenum pressure (correlated to the nozzle pressure), the plenum temperature, and the six load cells on the thrust stand. The data acquisition system sampled the input channels approximately once every 1.5 seconds.

The data was uploaded to a PC and imported into a spreadsheet program. The data was then averaged using a minimum of 20 data points. The spreadsheet calibrated out preprogrammed pressure effects generated in the plenum. The calibrated reactions were used to find the forces and moments for the three axis. The axial force was read directly from the force in the z-direction. The side and normal forces were read either directly from the forces in the x and y-directions or calculated from the moments about the x and y-axis. For the results in this report, the moments were used to generate the side and normal forces. The plenum and orifice plate data were used to generate measured and ideal weight flow rates and ideal axial thrust. Finally the pitch and yaw thrust vector angles were calculated using the axial, normal, and side forces. In addition to the forces, discharge coefficients, thrust coefficients and resultant thrust coefficients were calculated from the orifice, nozzle, and load cell data.

Results

The results for each data set are listed in Tables 3-6. For each vane configuration and NPR, the five computed performance parameters (F/F_i, F_r/F_i, w_p/w_i, δ_p, δ_i) are given. Graphs for the pitch thrust vector angle and yaw thrust vector angle are shown in Figures 3-6. Finally graphs representing the jet deflection turning angle envelope investigated in this report are presented in Figures 8 through 10. In addition, Figures 11a-14d, a total of 16 figures, are contained in Appendix A. These figures graph the thrust coefficient, resultant thrust coefficient, pitch trust vector angle and yaw thrust vector angle as a function of NPR similar to the format of reference 3.

Comparison of Cal Poly and NASA Results

Prior to collecting the data required for this report, a test run similar to one contained in NASA Technical Memorandum 4359 was performed. The vane configuration tested held the lower vane at -10 deg. while the upper and outer vanes were equally deployed into the flow. This test was run at NPR 5. Table 1 contains the data collected in this test and the data from Table 25 of TM4359. Figures 1a and 1b graph the yaw and pitch thrust vector angles presented in Table 1. These graphs show that the NASA and Cal Poly data show similar trends for the same vane configurations.

Table 2 contains data from TM4359 that can be directly compared to data collected for this report. This table shows that the maximum difference in compared data occurred for a vane configuration of (15,-10, 15) at NPR 5. The difference in the two sets of data at this point is .90 degrees pitch. The average difference between the data in Table 2, some 18 data point comparisons, is .35 degrees pitch and .34 degrees yaw. Since the scale of the Cal Poly and NASA test apparatus are different (4.17% for Cal Poly vs. 14.25% for NASA), some differences were expected. Tables 1 and 2 are intended to show approximately how close the two sets of data agree.

Nozzle Performance

For each data point, a discharge coefficient, w_p/w_i, a thrust coefficient, F/F_i, and a resultant thrust coefficient, F_r/F_i, are reported. In addition, For each data set the thrust and resultant thrust coefficients are plotted as a function of NPR and vane configuration. These graphs are included in Appendix A. There was very little change in the calculated discharge coefficient for all data points. The slight changes in the discharge coefficients appeared to be independent of NPR and vane configuration. Since the discharge coefficient depends on the internal geometry of the nozzle and is independent of any changes downstream from the throat, this result was expected. If, however, the throat of the nozzle became unchoked, it would be noted by a significant decrease in the w_p/w_i ratio. Both the axial thrust coefficient and the resultant thrust coefficient decrease with increasing jet deflection. As reported in NASA TM 4359, the axial thrust coefficient decreases due to the vane deflection diverting flow away from the axial direction. The resultant thrust coefficient decreases due to losses occurring from the interaction of the vanes and the supersonic flow.

Effects of Parametric Vane Deflection

The test envelope allows for two comparisons of the data sets to be made. The first comparison is of deploying the lower vane at a fixed setting, and comparing the different effects of deploying the upper vane with the outer vane held at -10 deg. or deploying the outer vane while the upper vane is held at -10 deg. This comparison can be better visualized by referring to figure 2. This comparison shows the differences that occur between configuration (a) and (c) and the differences between configuration (b) and (d). The second comparison examines the changes that occur between setting the fixed vane at 15 deg. vs. 10 deg. Again referring to figure 2, the second comparison shows the differences that occur between configuration (a) and (b) and the differences between configurations (c) and (d).

For the first comparison, refer to Tables 3 and 5 and Figures 3a, 3b, 5a, and 5b. For both these data sets the lower vane was set at 10 deg. The data in Table 3 corresponds to varying the upper vane while the outer vane was fully retracted. Table 5 corresponds to varying the outer vane while the upper vane was fully retracted. First examine the effects of varying the upper vane. Referring to Figures 3a and 3b, with the upper vane fully retracted, a positive yaw and

negative pitch thrust vector angle were present as a result of the lower vane deployed at 10 deg. As the upper vane was moved into the flow, the yaw resulting from the lower vane was decreased. However, as the upper vane was further deployed, it tended to deflect the jet into the lower vane resulting in an increase in the positive yaw thrust vector angle. This increase continued until at a setting of 25 deg. for the upper vane, the yaw thrust vector angle was greater than its initial value when the upper vane was set at -10 deg. The pitch thrust vector angle is initially negative when the upper vane is fully retracted. As the upper vane is deployed, the jet was deflected to a positive pitch thrust vector angle. The largest changes in the pitch thrust vector angle occurred in the settings between 10 and 20 deg. Beyond 20 deg., the effect of increasing pitch thrust vector angle vs. increasing upper vane deployment decreased as a result of the jet being deflected into the lower vane.

The results in Table 5 and Figures 5a and 5b were initially identical to those in Table 3 since both data sets start at the same vane configuration. However, the effects of deploying the outer vane are different than those for deploying the upper vane. Due to the smaller size of the outer vane and its closer angular positioning to the lower vane, the outer vane does not deflect the flow into the lower vane as was the case with the upper vane. As the outer vane was deployed, the yaw thrust vector angle was reversed from a positive value to a negative value. The pitch thrust vector angle, which starts negative, increases in the negative direction. The same results that apply to the comparison of configurations (a) and (c) also apply to configurations (b) and (d). Data for configurations (b) and (d) are listed in Tables 4 and 6 and are shown in Figures 4 and 6.

The second comparison looks at the changes that occur when the lower vane was deployed at 10 deg. vs. 15 deg. Configurations (a) and (b) will be compared. Looking at Figures 3a and 4a, the same characteristic yaw thrust vector angle loss and recovery occurred for both configurations. Configuration (b) showed an expected stronger yaw thrust vector angle do to the 15 deg. deployment of the lower vane. Figures 3b and 4b show that the pitch thrust vector angle for both configurations were almost identical. Initially configuration (b) showed an expected stronger pitch thrust vector angle due to the 15 deg. deployment of the lower vane, but as the upper vane was deployed into the flow the differences in magnitude between the two data sets decreased. The deployment of the lower vane at 10 deg. vs. 15 deg. had an effect on the magnitude of the resulting yaw thrust vector angle but did not effect the pitch thrust vector angle.

A comparison of configurations (c) and (d) can be made by examining Figures 5a, 5b, 6a, and 6b. These Figures show the same characteristic yaw and pitch curves for both sets of data.

6

The curves show different magnitudes of yaw and pitch depending on the deployment of the lower vane (10 deg. vs. 15 deg.).

NPR Effects

All vane configurations were tested at NPRs 3, 4, and 5. For a given vane configuration, all three NPRs tended to result in the same characteristic curve shape. However, the magnitudes of the thrust vector angle and in some cases the rates of change of the thrust vector angle curves were different for different NPRs.

Figures 3a and 4a show the larger yaw thrust vector angle resulting from the higher NPR. This can also be seen in Figures 3b and 4b for the pitch thrust vector angle. Both Figures 3 and 4 are for configurations where the larger upper vane was deployed at increasing vane settings into the flow while the outer vane was held at -10 deg. Figures 3 and 4 show the larger thrust vector angle for higher NPRs, but show only slight changes in the slope of the curves at different NPRs. These differences in the rate of change of the thrust vector angle are noticeable when the second vane was deployed at 0 deg. At this point, Figures 3 and 4 show that the slope of the thrust vector angle curves for NPRs 5 and 4 are starting to change with changing vane setting. The curve for NPR 3 does not show a change in slope at this point. As the second vane was further deployed into the flow, there are slight differences in the pitch thrust vector angle at 20 and 25 deg. Here the higher NPR curve tended to flatten out before the lower NPR curve. This resulted in the values of the pitch thrust vector angle at 25 deg. either being equal for all three NPRs or slightly greater for the lower NPR.

Figures 5 and 6 are for configurations where the smaller outer vane was deployed into the flow. These figures show that initially, the higher the NPR, the larger the thrust vector angle in both pitch and yaw. These figures also show that as the outer vane was deployed into the flow, the thrust vector angle curve at a NPR of 5 was much more responsive than the curve at NPR of 3. This resulted in a greater rate of change for the NPR 5 curve than for the NPR 3 curve. As the outer vane was further deployed into the flow, the curve for NPR 5 began to flatten out before the NPR 3 curve. This resulted in a greater rate of change for the NPR 3 curve than for the NPR 5 curve as the second vane was deployed through 20 and 25 deg. These results can also be seen in Figures 5b, 6a, and 6b. For the yaw thrust vector angle, this flattening of the curve was enough such that the lower NPR curves produced a larger thrust vector angle at 20 and 25 deg. In all these cases, the higher the NPR, the sooner a change in the thrust vector angle curve can be

noticed when a second vane was deployed into the flow. As the second vane was further deployed into the flow, the higher NPR curve tended to flatten out before the lower NPR curve.

The differences in rates of change of the curves can be attributed to the size of the exhaust jet plume at different NPRs. Figure 7 shows three Schlieren photographs of the Cal Poly cold flow nozzle with a single vane attached. The three photographs are for NPRs of 3, 4, and 5. These photographs show that the size of the exhaust jet plume increased with increasing NPR. When a second vane was deployed into the flow, the larger exhaust plume associated with the higher NPR tended to be effected first. This can be seen in all the figures where the slope of thrust vector angle changed first at the higher NPRs.

The second region where there was a difference in slope for different NPRs was at a deployment position of 20 and 25 deg. for the second vane. This difference occurred most noticeably for the case when the second vane being deployed was the smaller outer vane (Figures 5 and 6), and to a lesser extent when the larger upper vane (Figures 3 and 4) was the second vane being deployed. This effect was again a result of the size of the exhaust plume and also the size of the second vane being deployed. At large settings of the smaller second vane, much of the exhaust plume expanded around the vane. This decreased the effectiveness of the vanes ability to turn the flow. For higher NPRs, the larger exhaust plume increased this ineffectiveness of the second vanes turning potential. This resulted in the second vane having a greater effect on turning the lower NPR flow than the higher NPR flow. In the case of the larger upper vane being deployed into the flow, the expansion of the jet plume around the vane was less significant. Thus, at large settings of the upper vane, the slopes of the thrust vector angles are much closer for all NPRs.

Thrust Vectoring Envelope

The thrust vectoring envelopes created by combining all the test data are graphed in Figures 8, 9, and 10. Results are presented as δ_p plotted against δ_y for a given NPR. Each graph presents the resulting δ_p and δ_y achieved when the lower vane is deployed at 10 deg. and 15 deg. and either the upper or outer vane is deployed into the flow.

The graphs show that pitch vectoring capability exceeds the yaw vectoring ability for the test envelope. In addition, there are both pure pitch and pure yaw vector angles present. A pure pitch vector angle occurs when the set of data points graphed in Figures 8, 9, and 10 crosses through a zero deg. yaw angle value at a non zero deg. pitch angle value. Likewise, a pure yaw

angle occurs when the data points cross through a zero deg. pitch angle for a non zero deg. yaw angle.

The graphs also show the higher the value of the NPR, the larger the pitch and yaw thrust vector angles. The exception to this is at points where the second vane was fully deployed into the flow and the higher NPR curves began to flatten out.

Conclusions

A cold jet test program was conducted on the 1/24th scale single flow thrust vectoring model at Cal Poly University. The test envelope consisted of prescribed vane configurations requested by NASA. The vane configurations were tested at NPRs 3, 4, and 5. The results presented in this report led to the following conclusions:

1. Some of the data in this report can be directly compared to NASA data for the same vane configuration and NPR. In some cases the values of this data differ, but the difference is small (.35 deg. pitch and .34 deg. yaw) and the data comparison indicates the same trends.

2. For a given vane configuration, different NPRs led to different values of jet turning angles but follow the same characteristic trends.

3. When the lower vane was deployed at a fixed setting (10 deg. or 15 deg.), the effects of deploying a second vane into the flow depends on which vane was deployed. If the upper vane was deployed, at large vane settings the exhaust stream was deflected off the upper vane back into the lower vane resulting in a recovery of the yaw thrust vector angle. If the smaller outer vane was deployed, this did not occur. In this case the exhaust stream was deflected away from the nozzle primarily by the outer vane.

4. In general, for a given vane configuration, the higher the value of the NPR, the larger the magnitude of the thrust vector angle. The exception to this was at points where the second vane was deployed at the 20 and 25 deg. region. In this region, some of the higher NPR thrust vector angle curves tended to flatten out, resulting in the lower NPR having a greater thrust vector angle than the higher NPR. This was the case for configurations (a) and (b) in the pitch thrust vector angle, and for configurations (c) and (d) for the yaw thrust vector angle.

5. The pitch turning capability exceeded the yaw turning capability for the test envelope in this report. The range of pitch thrust vector angle achieved by the configurations tested was between -12 deg. and 12 deg. For the yaw thrust vector angle, the range was between -5 deg. and 6 deg. In addition, both pure pitch and pure yaw angles were present allowing for isolated moments.

References

1.   Bowers, Albion H.; Noffz, Gregory K.; Grafton, Sue B.; Mason , Mary L.; Peron, Lee R.; Multiaxis Thrust Vectoring Using Axisymmetric Nozzles and Postexit Vanes on an F/A-18 Configuration Vehicle; April 1991

2.   Carpenter, Thomas W.; Vaccarezza, Stephen E., Dobbins, Sean W.; Design and Evaluation of Single and Dual Flow Thrust Vector Nozzles With Post Exit Vanes, Semi-Annual Progress Report, NASA-AMES Grant Number NCC2-748; April 1993

3.   NASA Technical Memorandum 4359
June 1992

Table 1.   Comparison of Experimental Data from Cal Poly 1/24 Scale Model with that
            Presented in Table 25 of the NASA TM 4359-A Static Investigation of the Thrust
            Vectoring System of the F/A-18 High-Alpha Research Vehicle. Vanes A and B
            Deployed and Vane B Fully retracted where NPR=5

[δ_p and δ_y are given in degrees]

	$\delta_A=0°$	$\delta_B=0°$	$\delta_C=-10°$	
	NASA		Cal Poly	
NPR	δ_p	δ_y	δ_p	δ_y
5	0.60	-0.37	0.49	-0.31

	$\delta_A=10°$	$\delta_B=10°$	$\delta_C=-10°$	
	NASA		Cal Poly	
NPR	δ_p	δ_y	δ_p	δ_y
5	3.70	-3.68	3.23	-3.77

	$\delta_A=20°$	$\delta_B=20°$	$\delta_C=-10°$	
	NASA		Cal Poly	
NPR	δ_p	δ_y	δ_p	δ_y
5	10.14	-12.07	8.70	-10.60

	$\delta_A=30°$	$\delta_B=30°$	$\delta_C=-10°$	
	NASA		Cal Poly	
NPR	δ_p	δ_y	δ_p	δ_y
5	14.37	-18.25	13.60	-18.55

12

Table 2.   Comparison of Experimental Data from Cal Poly with that Presented in the NASA TM 4359-A Static Investigation of the Thrust Vectoring System of the F/A-18 High-Alpha Research Vehical

[δ_p and δ_y are given in degrees]

NASA Table Ref.	NPR	δ_A=-10° δ_B=-10° δ_C=10°					
		NASA		Cal Poly			
		δ_p	δ_y	δ_p	δ_y	$\Delta\delta_p$	$\Delta\delta_y$
23	3	-0.78	1.24	-0.82	1.00	0.40	0.24
	4	-1.64	2.12	-1.61	2.02	0.03	0.10
	5	-2.57	3.01	-2.38	2.85	0.19	0.16

NASA Table Ref.	NPR	δ_A=-10° δ_B=-10° δ_C=15°					
		NASA		Cal Poly			
		δ_p	δ_y	δ_p	δ_y	$\Delta\delta_p$	$\Delta\delta_y$
23	3	-2.44	3.09	-2.54	3.09	0.10	0.00
	4	-3.31	3.90	-3.27	3.78	0.04	0.12
	5	-4.24	4.71	4.71	4.31	0.52	0.40

NASA Table Ref.	NPR	δ_A=-10° δ_B=10° δ_C=10°					
		NASA		Cal Poly			
		δ_p	δ_y	δ_p	δ_y	$\Delta\delta_p$	$\Delta\delta_y$
27	3	-1.95	-0.15	-1.58	0.05	0.37	0.20
	4	-3.24	-0.23	-2.92	0.02	0.32	0.25
	5	-4.88	-0.37	-4.58	-0.06	0.30	0.31

13

Table 2. (Continued)

NASA Table Ref.	NPR	δ_A=-10° δ_B=15° δ_C=15° NASA		Cal Poly			
		δ_p	δ_y	δ_p	δ_y	$\Delta\delta_p$	$\Delta\delta_y$
27	3	-5.91	-0.56	-5.27	0.12	0.64	0.68
	4	-7.18	-0.64	-6.69	-0.31	0.49	0.49
	5	-8.57	-0.75	-7.71	-0.31	0.86	0.44

NASA Table Ref.	NPR	δ_A=10° δ_B=-10° δ_C=10° NASA		Cal Poly			
		δ_p	δ_y	δ_p	δ_y	$\Delta\delta_p$	$\Delta\delta_y$
29	3	1.50	1.23	1.12	0.94	0.38	0.29
	4	2.14	1.88	1.87	1.56	0.27	0.32
	5	3.00	2.62	2.80	2.21	0.20	0.41

| NASA Table Ref.	NPR	δ_A=15° δ_B=-10° δ_C=15° NASA		Cal Poly			
		δ_p	δ_y	δ_p	δ_y	$\Delta\delta_p$	$\Delta\delta_y$
29	3	3.64	3.30	3.73	2.92	0.09	0.38
	4	4.55	3.98	4.01	3.31	0.54	0.67
	5	5.27	4.36	4.72	3.46	0.55	0.90

14

Table 3. Performance of a 1/24 Scale Model Maximum A/B-Power Nozzle with Rotating Vane System for a Large Vane and Two Standard Vanes with Vanes A and C deployed and Vane B Fully Retracted.

[δ_p and δ_y are given in degrees]
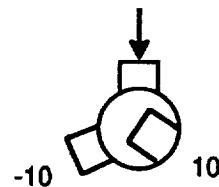
NPR	$\delta_A=-10°$ w_p/w_i	$\delta_B=-10°$ F/F_i	$\delta_C=10°$ F_r/F_i	δ_p	δ_y
3.010	.972	.959	.959	-0.93	1.24
3.990	.970	.945	.946	-1.76	2.07
4.984	.939	.927	.929	-2.47	2.89

NPR	$\delta_A=0°$ w_p/w_i	$\delta_B=-10°$ F/F_i	$\delta_C=10°$ F_r/F_i	δ_p	δ_y
3.011	0.968	0.965	0.965	-0.98	1.32
3.989	0.974	0.950	0.951	-1.65	2.04
4.984	0.939	0.940	0.941	-1.80	2.76

NPR	$d_A=5°$ w_p/w_i	$\delta_B=-10°$ F/F_i	$\delta_C=10°$ F_r/F_i	δ_p	δ_y
3.010	0.974	0.955	0.955	-0.57	1.16
3.990	0.975	0.945	0.945	-0.48	1.87
4.986	0.943	0.931	0.931	-0.01	2.50

NPR	$\delta_A=10°$ w_p/w_i	$\delta_B=-10°$ F/F_i	$\delta_C=10°$ F_r/F_i	δ_p	δ_y
3.010	0.967	0.934	0.935	1.12	0.94
3.990	0.975	0.928	0.929	1.87	1.56
4.986	0.980	0.894	0.895	2.80	2.21

15

Table 3. (Continued)
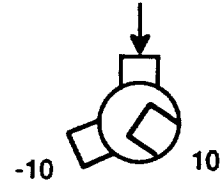
NPR	$\delta_A=15°$ w_p/w_i	$\delta_B=-10°$ F/F_i	$\delta_C=10°$ F_r/F_i	δ_p	δ_y
3.010	0.962	0.912	0.915	4.37	0.77
3.990	0.976	0.908	0.912	4.97	1.24
4.982	0.970	0.888	0.839	5.57	1.99

NPR	$\delta_A=20°$ w_p/w_i	$\delta_B=-10°$ F/F_i	$\delta_C=10°$ F_r/F_i	δ_p	δ_y
3.010	0.969	0.861	0.869	7.65	1.11
3.991	0.973	0.878	0.886	7.74	1.67
4.982	0.977	0.862	0.872	8.17	2.26

NPR	$\delta_A=25°$ w_p/w_i	$\delta_B=-10°$ F/F_i	$\delta_C=10°$ F_r/F_i	δ_p	δ_y
3.010	0.975	0.816	0.830	10.63	1.92
3.990	0.968	0.828	0.842	10.34	2.62
4.985	0.973	0.834	0.849	10.11	3.15

Table 4.   Performance of a 1/24 Scale Model Maximum A/B-Power Nozzle with Rotating Vane System for a Large Vane and Two Standard Vanes With Vanes A and C Deployed and Vane B Fully Retracted.

[δ_p and δ_y are given in degrees]
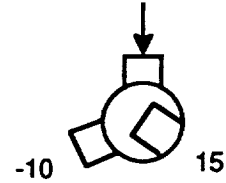
	$\delta_A = -10°$	$\delta_B = -10°$	$\delta_C = 15°$		
NPR	w_p/w_i	F/F_i	F_r/F_i	δ_p	δ_y
2.999	0.967	0.937	0.939	-2.55	3.09
3.999	0.971	0.929	0.932	-3.27	3.78
5.012	0.972	0.932	0.937	-3.72	4.31

	$\delta_A = 0°$	$\delta_B = -10°$	$\delta_C = 15°$		
NPR	w_p/w_i	F/F_i	F_r/F_i	δ_p	δ_y
3.099	0.982	0.938	0.941	-2.57	3.11
3.992	0.973	0.929	0.932	-3.19	3.72
5.011	0.973	0.928	0.932	-3.23	4.28

	$\delta_A = 5°$	$\delta_B = -10°$	$\delta_C = 15°$		
NPR	w_p/w_i	F/F_i	F_r/F_i	δ_p	δ_y
3.000	0.972	0.927	0.929	-2.17	2.97
3.992	0.978	0.923	0.925	-1.54	3.58
5.011	0.971	0.931	0.934	-0.84	4.28

	$\delta_A = 10°$	$\delta_B = -10°$	$\delta_C = 15°$		
NPR	w_p/w_i	F/F_i	F_r/F_i	δ_p	δ_y
3.000	0.964	0.921	0.922	0.07	2.81
3.992	0.972	0.909	0.911	0.37	3.34
5.012	0.972	0.896	0.899	1.50	3.78

17

Table 4. (Continued)
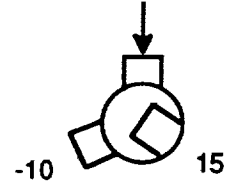
NPR	$\delta_A=15°$ w_p/w_i	$\delta_B=-10°$ F/F_i	$\delta_C=15°$ F_r/F_i	δ_p	δ_y
3.000	0.977	0.865	0.868	3.73	2.92
3.999	0.977	0.876	0.879	4.01	3.31
5.011	0.968	0.889	0.893	4.73	3.46

NPR	$\delta_A=20°$ w_p/w_i	$\delta_B=-10°$ F/F_i	$\delta_C=15°$ F_r/F_i	δ_p	δ_y
3.000	0.986	0.848	0.855	6.71	3.30
3.993	0.975	0.838	0.846	6.64	3.85
5.010	0.971	0.837	0.847	7.73	4.08

NPR	$\delta_A=25°$ w_p/w_i	$\delta_B=-10°$ F/F_i	$\delta_C=15°$ F_r/F_i	δ_π	δ_ψ
3.000	0.966	0.793	0.807	9.55	4.51
3.993	0.969	0.811	0.797	9.48	5.07
5.014	0.974	0.793	0.808	9.62	5.10

Table 5. Performance of a 1/24 Scale Model Maximum A/B-Power Nozzle with Rotating Vane System for a Large Vane and Two Standard Vanes with Vanes B and C Deployed and Vane A Fully Retracted.

[δ_p and δ_y are given in degrees]   -10

10
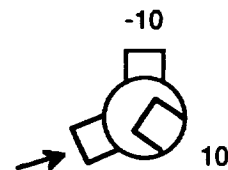
NPR	δ_A=-10° w_p/w_i	δ_B=-10° F/F$_i$	δ_C=10° F$_r$/F$_i$	δ_p	δ_y
2.997	0.966	0.957	0.958	-0.82	1.00
3.988	0.973	0.959	0.960	-1.62	2.03
4.998	0.975	0.953	0.955	-2.38	2.85

NPR	δ_A=-10° w_p/w_i	δ_B=0° F/F$_i$	δ_C=10° F$_r$/F$_i$	δ_p	δ_y
2.998	0.967	0.961	0.961	-0.83	0.93
3.987	0.973	0.964	0.964	-1.59	1.96
4.997	0.974	0.959	0.961	-2.51	2.63

NPR	δ_A=-10° w_p/w_i	δ_B=5° F/F$_i$	δ_C=10° F$_r$/F$_i$	δ_p	δ_y
2.998	0.966	0.950	0.950	-0.90	0.89
3.986	0.973	0.958	0.959	-1.98	1.45
4.998	0.971	0.929	0.931	-3.52	1.56

NPR	δ_A=-10° w_p/w_i	δ_B=10° F/F$_i$	δ_C=10° F$_r$/F$_i$	δ_p	δ_y
2.998	0.967	0.929	0.929	-1.58	0.05
3.999	0.973	0.949	0.950	-2.92	0.02
4.998	0.973	0.926	0.929	-4.58	-0.06

19

Table 5. (Continued)
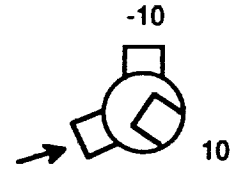
NPR	$\delta_A=-10°$ w_p/w_i	$\delta_B=15°$ F/F_i	$\delta_C=10°$ F_r/F_i	δ_p	δ_y
2.998	0.963	0.926	0.927	-3.00	-1.66
3.990	0.970	0.929	0.932	-4.37	-1.82
4.997	0.974	0.900	0.906	-6.05	-1.89

NPR	$\delta_A=-10°$ w_p/w_i	$\delta_B=20°$ F/F_i	$\delta_C=10°$ F_r/F_i	δ_p	δ_y
2.997	0.966	0.909	0.914	-4.97	-3.27
3.990	0.975	0.912	0.918	-6.33	-2.96
4.997	0.977	0.890	0.899	-7.78	-2.75

NPR	$\delta_A=-10°$ w_p/w_i	$\delta_B=25°$ F/F_i	$\delta_C=10°$ F_r/F_i	δ_p	δ_y
2.997	0.975	0.853	0.864	-8.01	-4.24
3.984	0.969	0.875	0.888	-9.05	-3.58
4.999	0.972	0.863	0.878	-9.96	-3.14

Table 6. Performance of a 1/24 scale Model Maximum A/B-Power Nozzle with Rotating Vane System for a Large Vane and Two Standard Vanes with Vanes B and C deployed and Vane A Fully Retracted.

[δ_p and δ_y are given in degrees]

-10

15
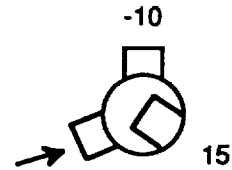
	δ_A=-10°	δ_B=-10°	δ_C=15°		
NPR	w_p/w_i	F/F_i	F_r/F_i	δ_p	δ_y
3.000	0.970	0.952	0.954	-2.51	2.95
3.986	0.969	0.957	0.960	-3.25	3.71
5.023	0.978	0.928	0.933	-3.88	4.54

	δ_A=-10°	δ_B=0°	δ_C=15°		
NPR	w_p/w_i	F/F_i	F_r/F_i	δ_p	δ_y
3.001	0.968	0.926	0.929	-2.68	3.08
3.987	0.969	0.937	0.940	-3.35	3.79
5.021	0.974	0.929	0.929	-4.08	4.34

	δ_A=-10°	δ_B=5°	δ_C=15°		
NPR	w_p/w_i	F/F_i	F_r/F_i	δ_p	δ_y
3.001	0.974	0.925	0.927	-2.63	2.76
3.986	0.970	0.939	0.934	-3.82	3.06
5.023	0.971	0.928	0.933	-4.75	3.22

	δ_A=-10°	δ_B=10°	δ_C=15°		
NPR	w_p/w_i	F/F_i	F_r/F_i	δ_p	δ_y
3.001	0.969	0.912	0.914	-3.49	1.85
3.998	0.963	0.935	0.938	-4.62	1.81
5.023	0.969	0.914	0.920	-5.98	1.51

21

Table 6. (Continued)
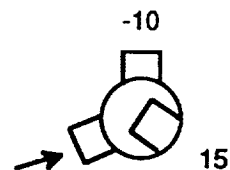
NPR	$\delta_A=-10°$ w_p/w_i	$\delta_B=15°$ F/F_i	$\delta_C=15°$ F_r/F_i	δ_p	δ_y
3.001	0.972	0.911	0.915	-5.27	0.12
3.987	0.955	0.930	0.937	-6.69	-0.31
5.023	0.975	0.888	0.896	-7.71	-0.31

NPR	$\delta_A=-10°$ w_p/w_i	$\delta_B=20°$ F/F_i	$\delta_C=15°$ F_r/F_i	δ_p	δ_y
3.003	0.969	0.893	0.901	-7.66	-1.28
3.986	0.967	0.872	0.884	-9.33	-1.35
5.022	0.977	0.864	0.877	-9.90	-1.26

NPR	$\delta_A=-10°$ w_p/w_i	$\delta_B=25°$ F/F_i	$\delta_C=15°$ F_r/F_i	δ_p	δ_y
3.003	0.964	0.847	0.863	-10.80	-2.17
3.987	0.969	0.848	0.866	-11.50	-1.89
5.024	0.978	0.831	0.850	-12.20	-1.88
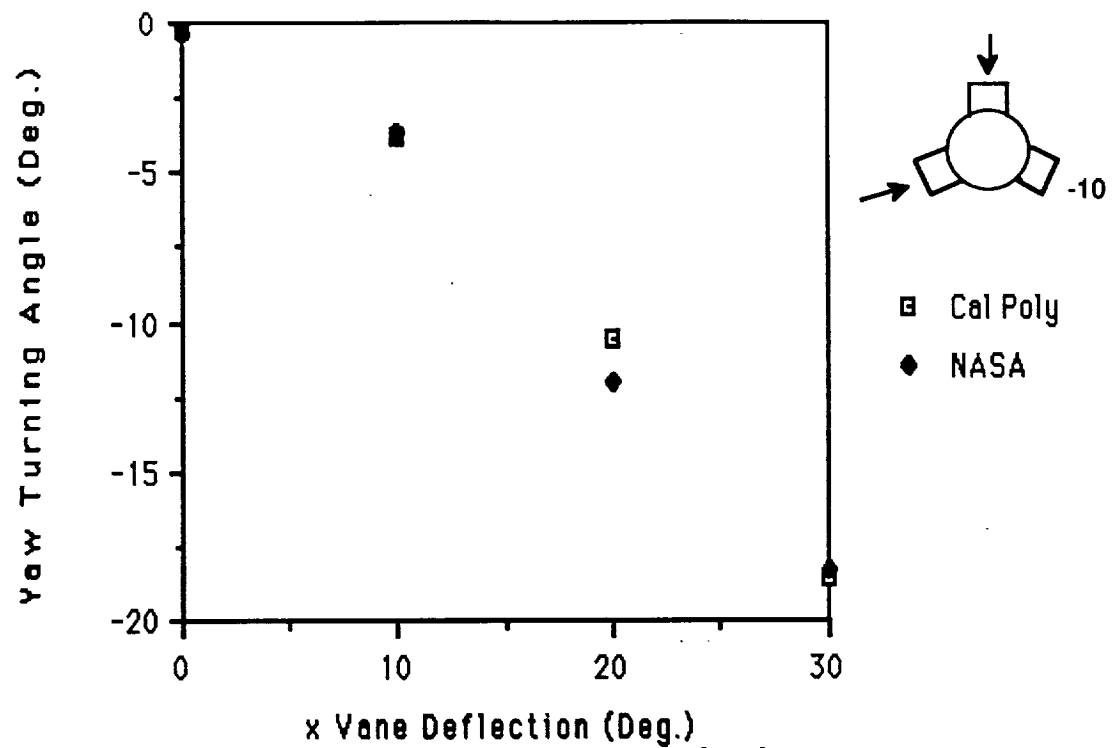
Figure 2a. Yaw Thrust Vector Angle
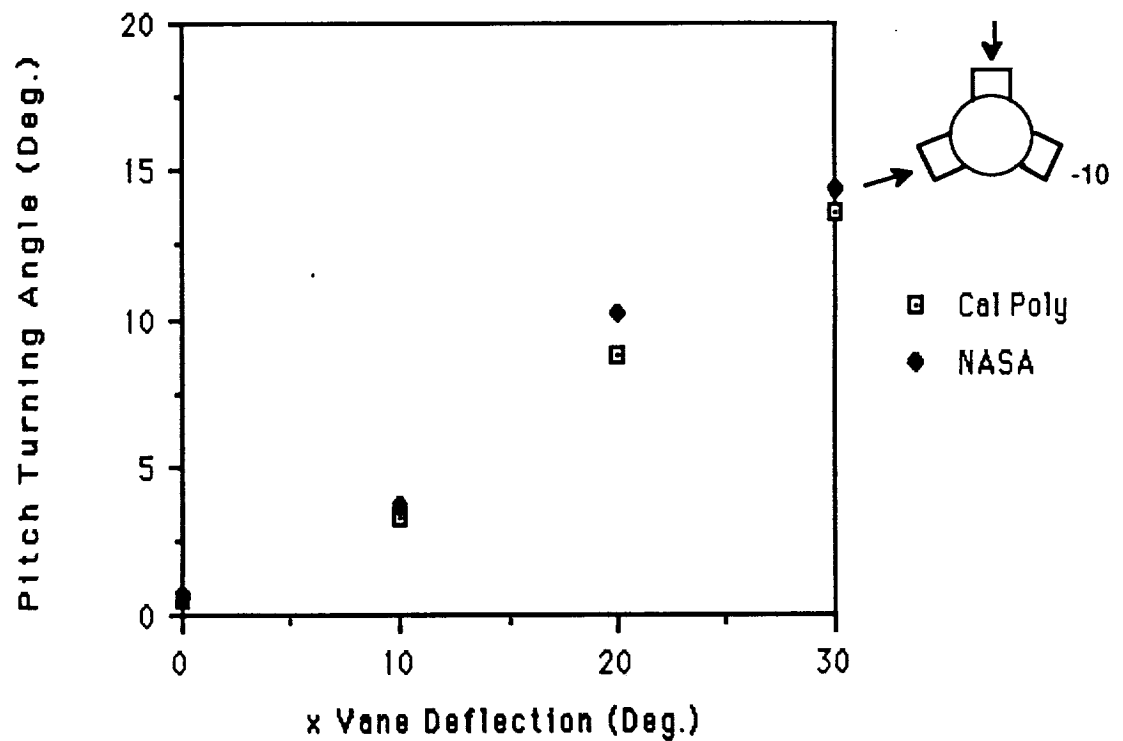
Figure 2b. Pitch Thrust Vector Angle

Figure 2. Cal Poly-NASA Thrust Vector Performance Comparison For Maximum A/B-Power Nozzle with Vanes A and B Equally Deployed and Vane C Retracted

23

-10°,0°,5°, 10°,15°,20°,25°

A

C

B

-10°   10°

Configuration (a)

-10°,0°,5°, 10°,15°,20°,25°

A

C

B

-10°   15°

Configuration (b)

-10°

A

C

B

-10°,0°,5°, 10°,15°,20°,25°   10°

Configuration (c)

-10°

A

C

B

-10°,0°,5°, 10°,15°,20°,25°   15°

Configuration (d)
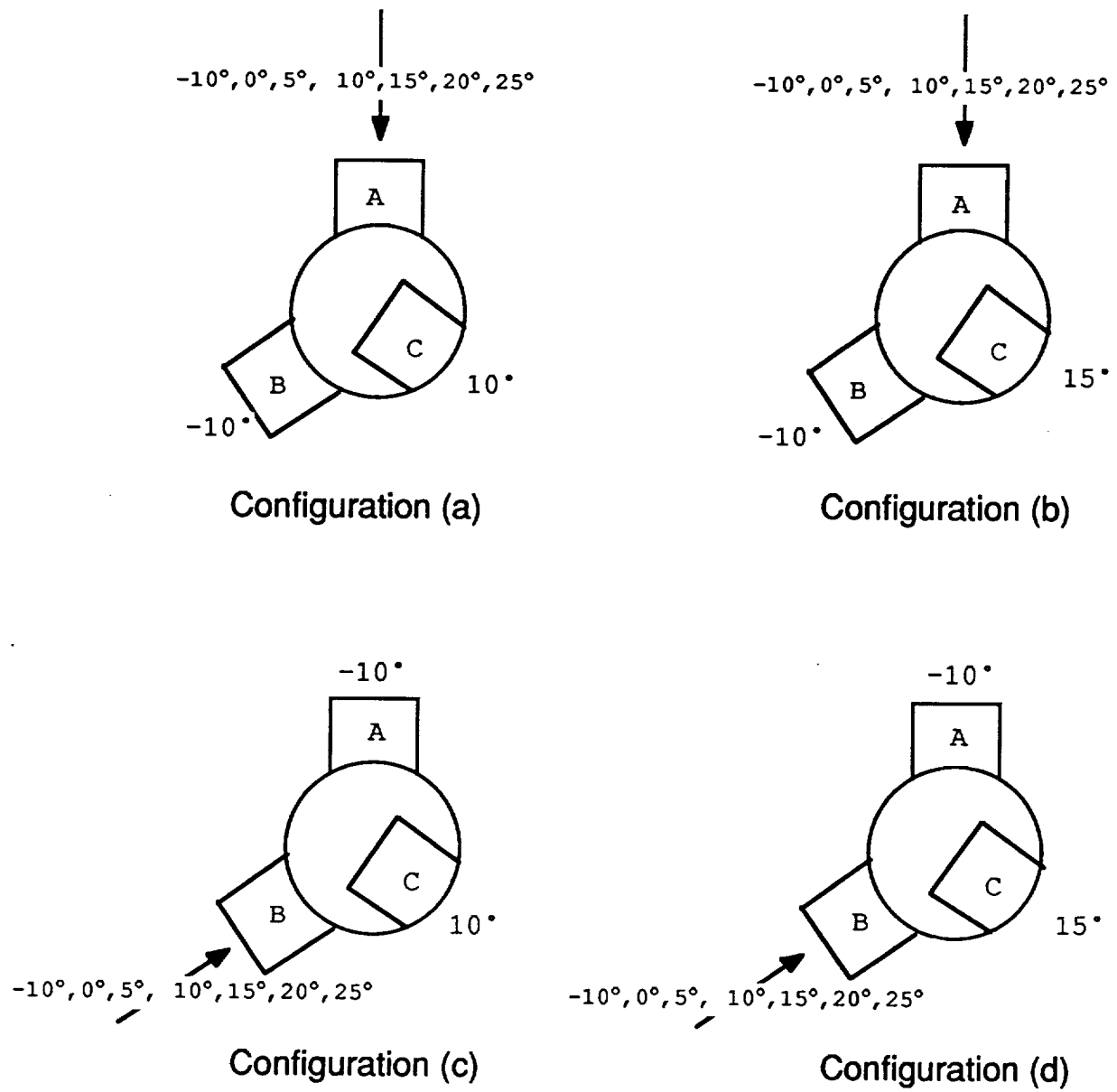
Figure 2. Test Envelope
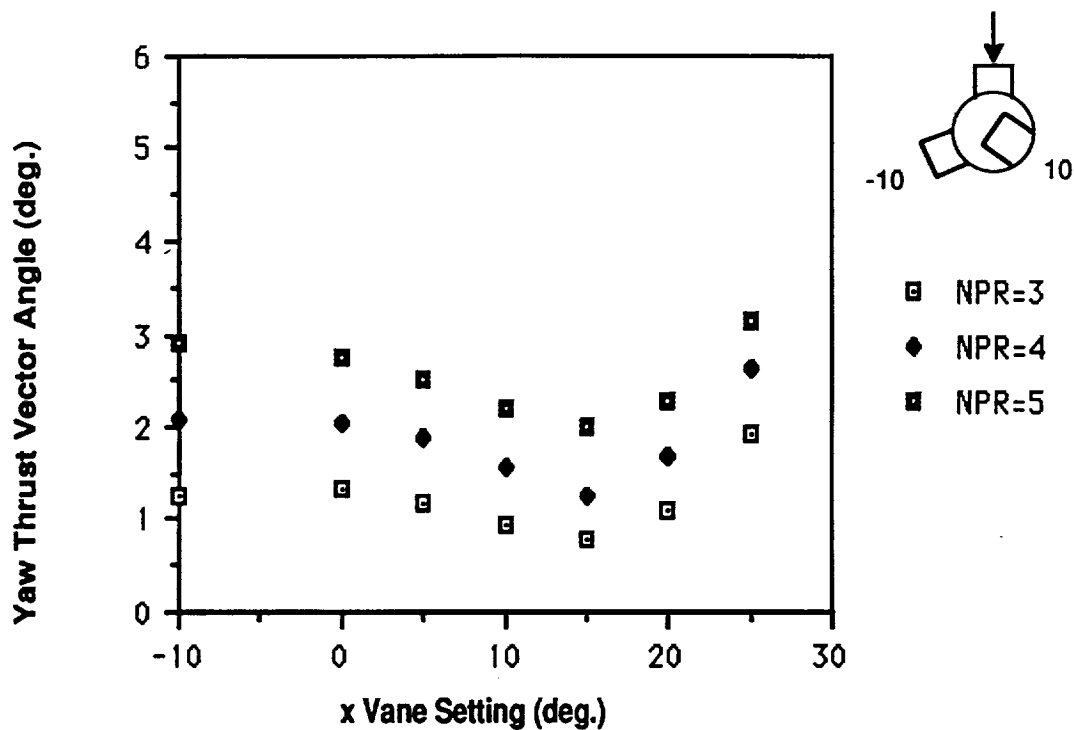
Figure 3a. Yaw Thrust Vector Angle
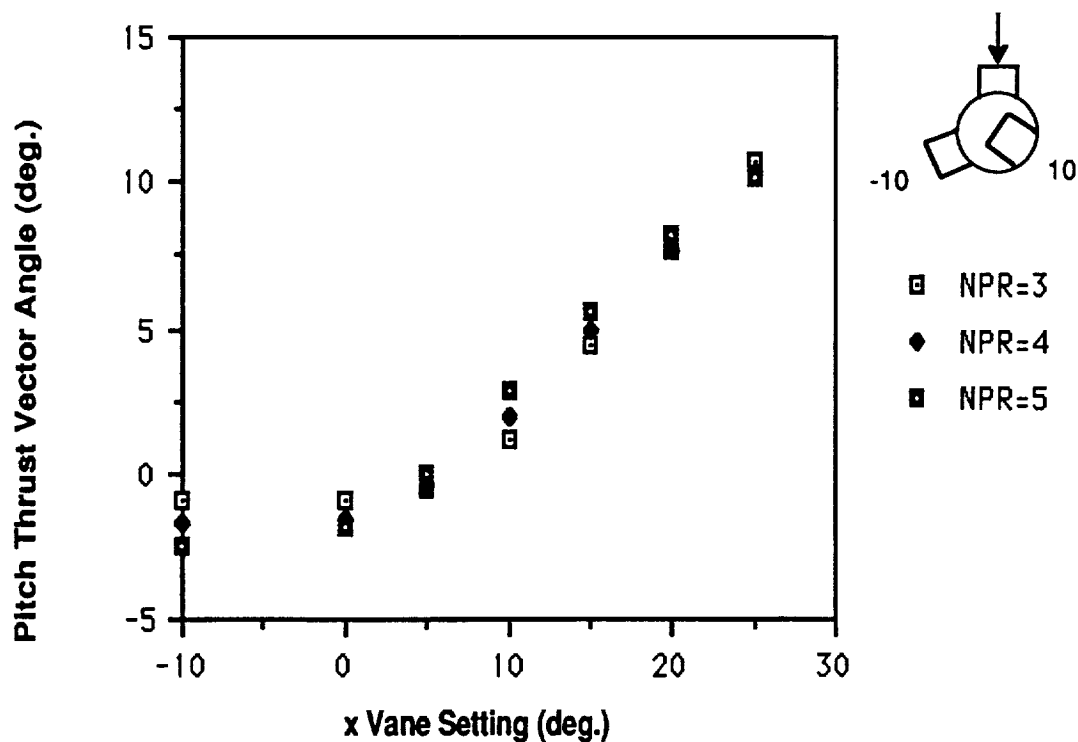
Figure 3b. Pitch Thrust Vector Angle

Figure 3. Thrust Vector Performance For Maximum A/B-Power Nozzle with
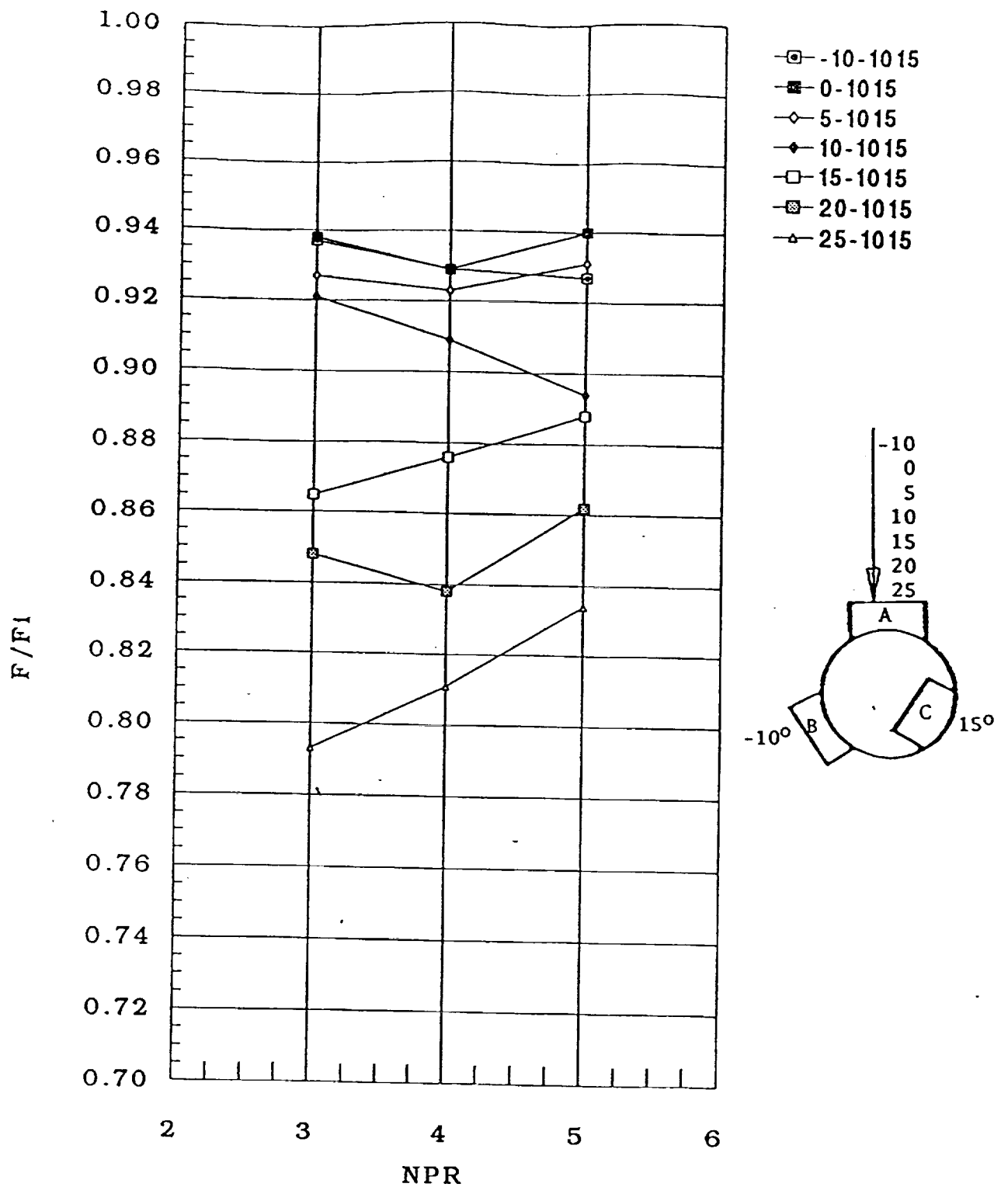Vanes A and C Deployed and Vane B Retracted
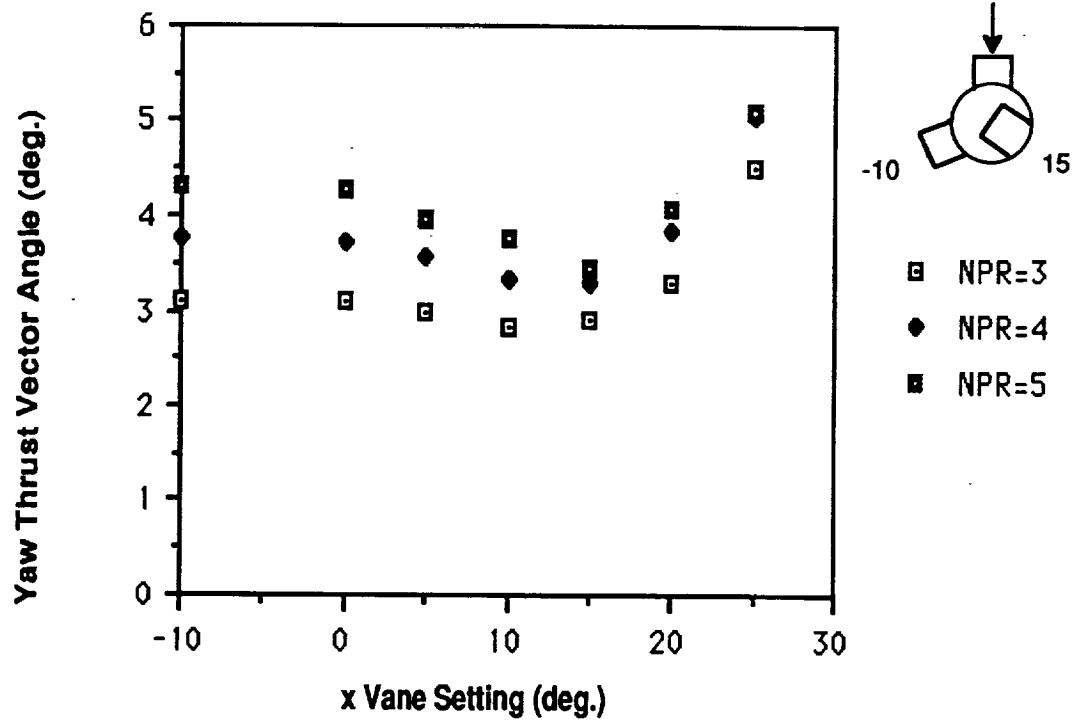
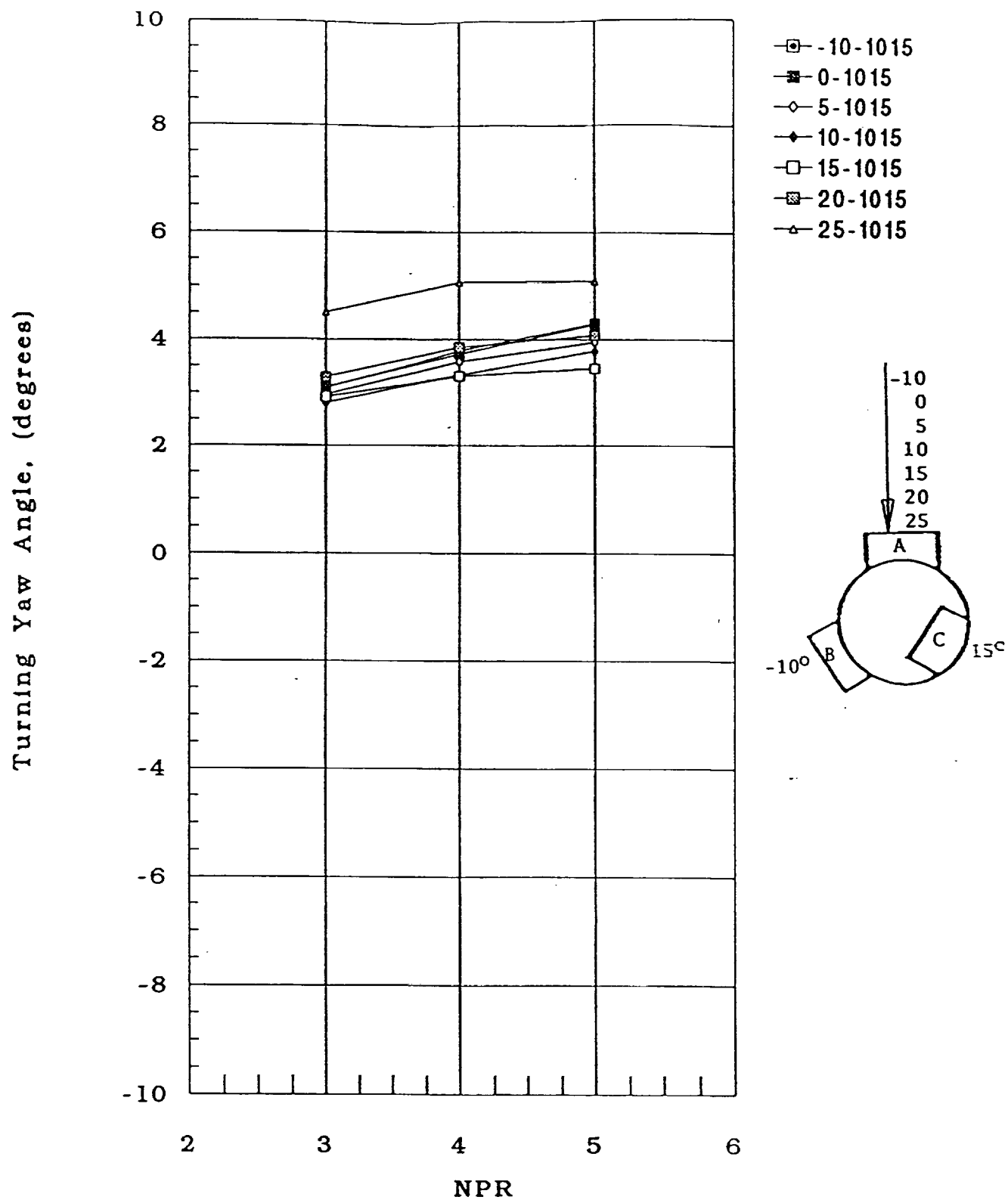Figure 4a. Yaw Thrust Vector Angle
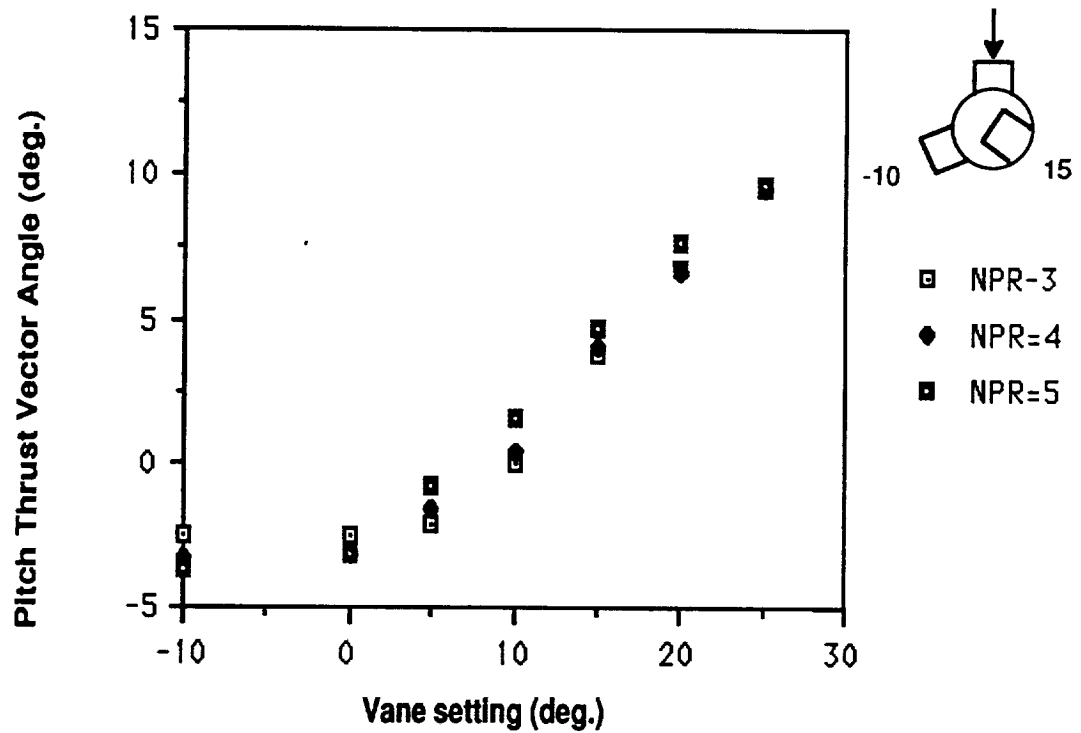
Figure 4b. Pitch Thrust Vector Angle

Figure 4. Thrust Vector Performance For Maximum A/B-Power Nozzle with
Vanes A and C Deployed and Vane B Retracted

26
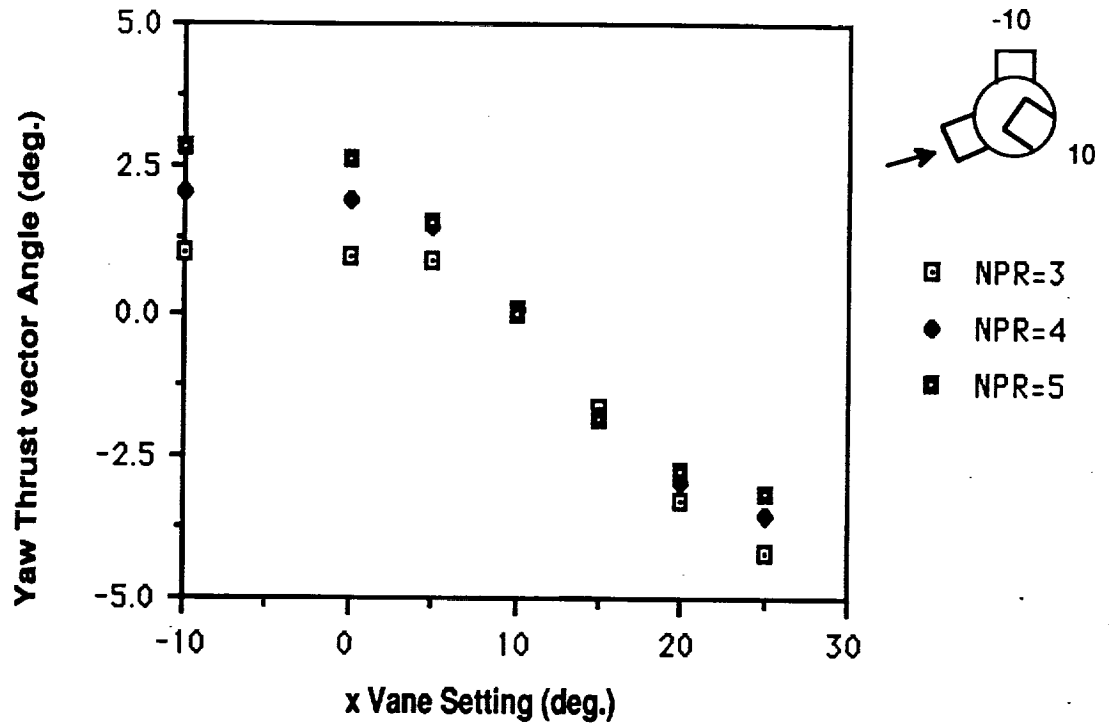
Figure 5a. Yaw Thrust Vector Angle
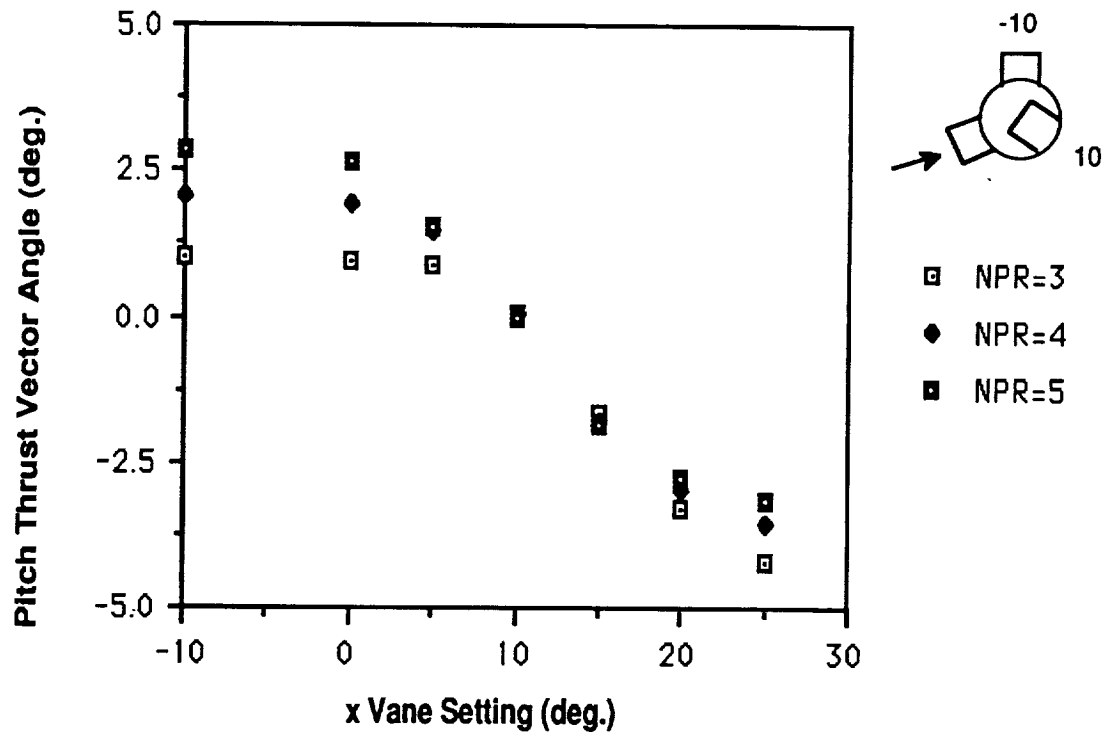
Figure 5b. Pitch Thrust Vector Angle
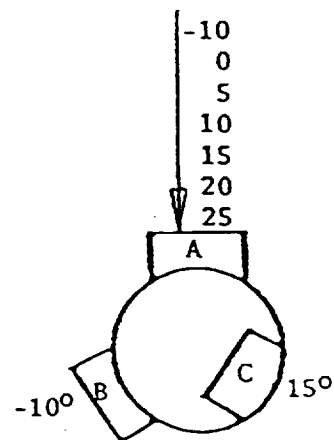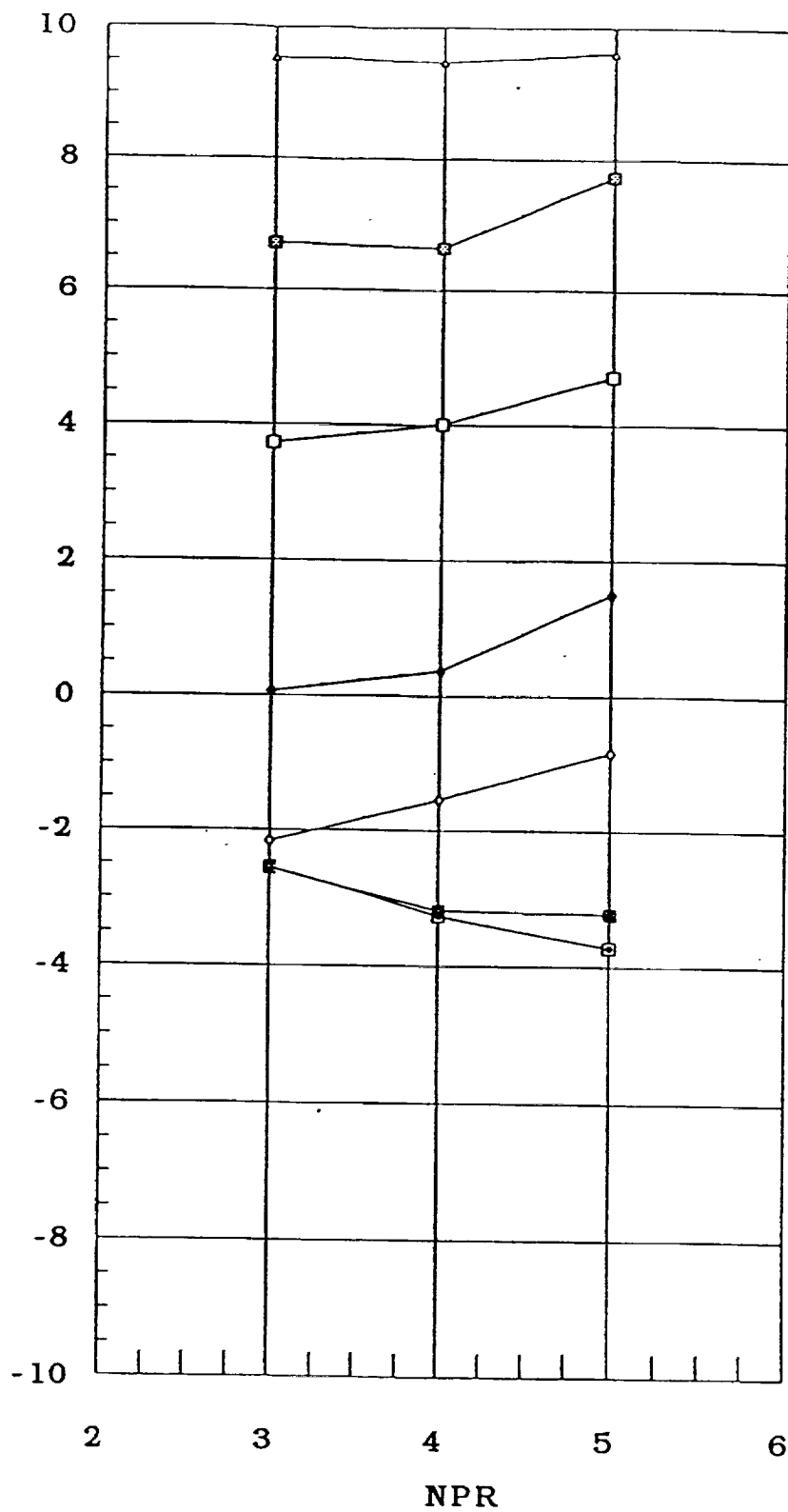
Figure 5. Thrust Vector Performance For Maximum A/B-Power Nozzle with
Vanes B and C Deployed and Vane B retracted
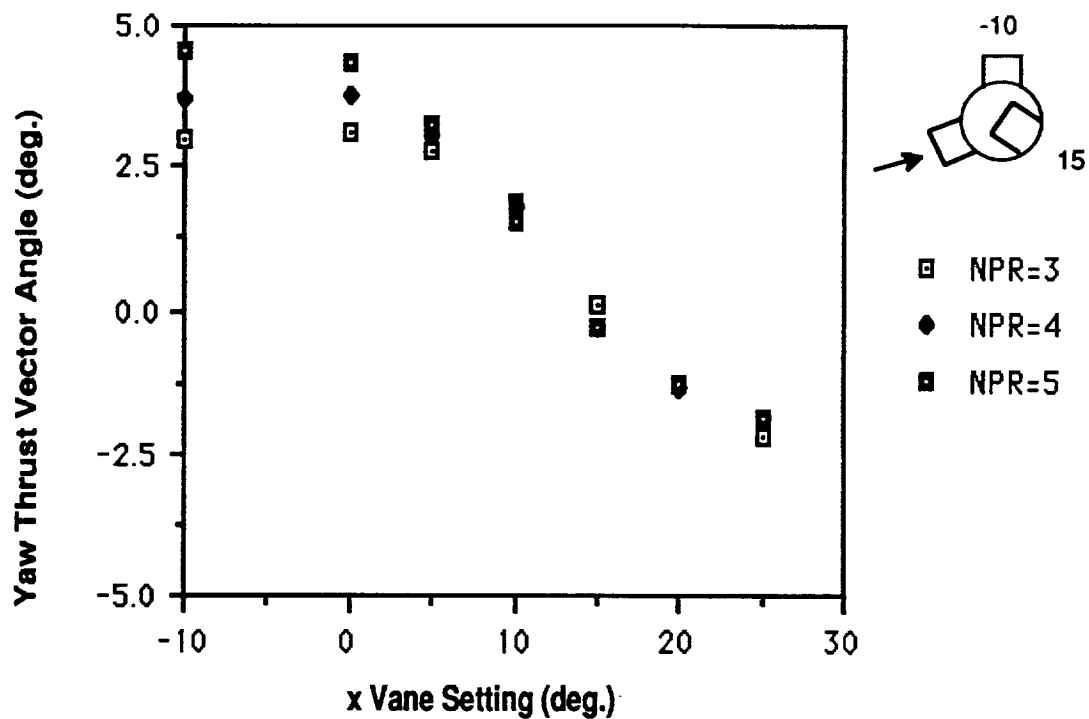
Figure 6a. Yaw Thrust Vector Angle
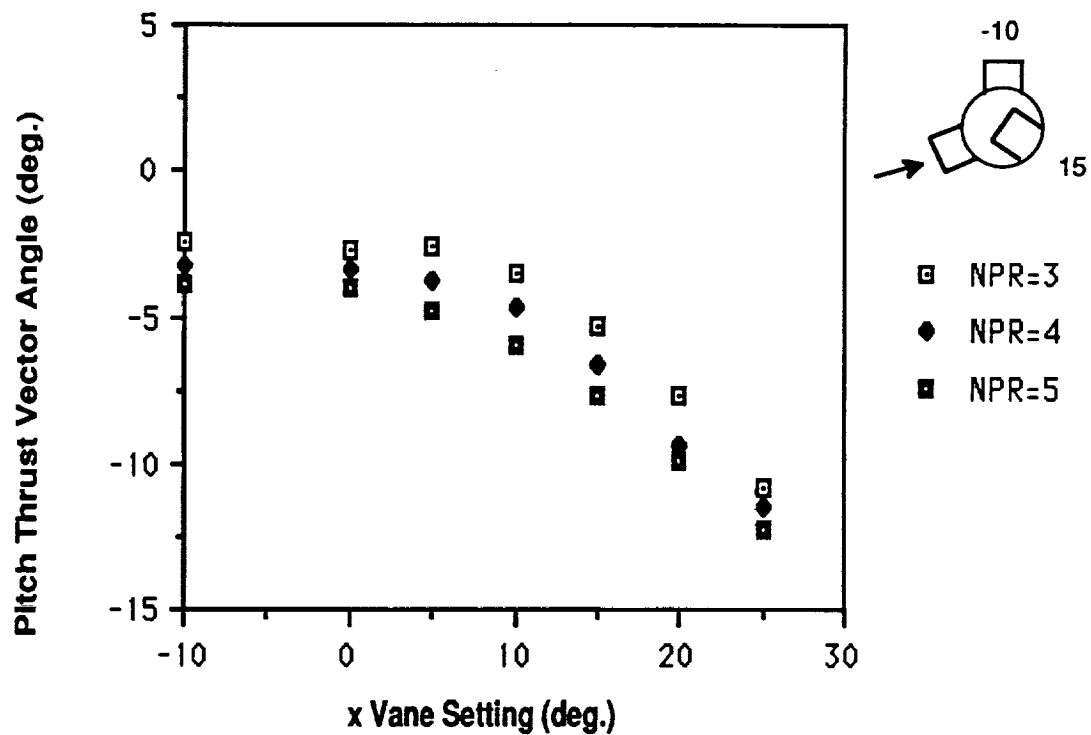
Figure 6b. Pitch Thrust Vector Angle

Figure 6. Thrust Vector Performance For Maximum A/B-Power Nozzle with
Vanes B and C Deployed and Vanes A Retracted

28
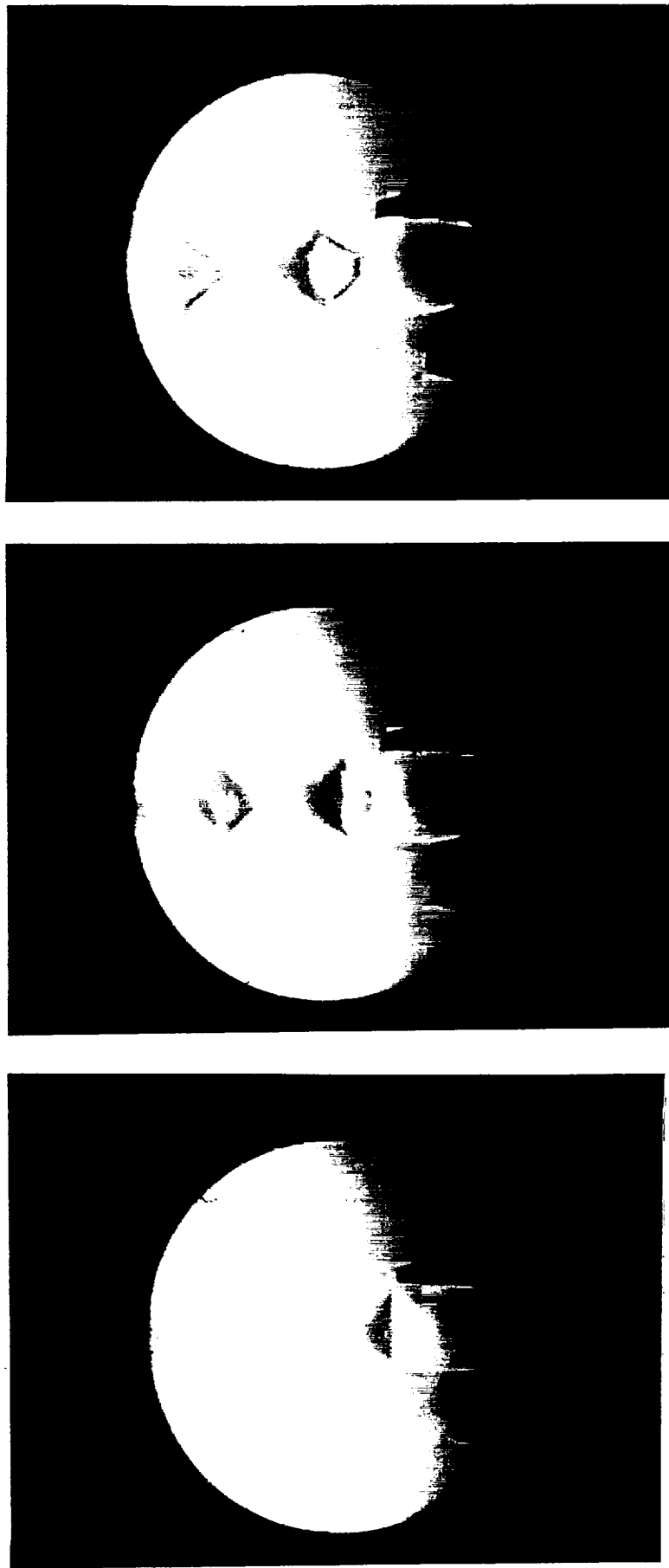
Figure 7. Schlieren photographs of an underexpanded nozzle. From left to right, NPRs 3, 4, and5.
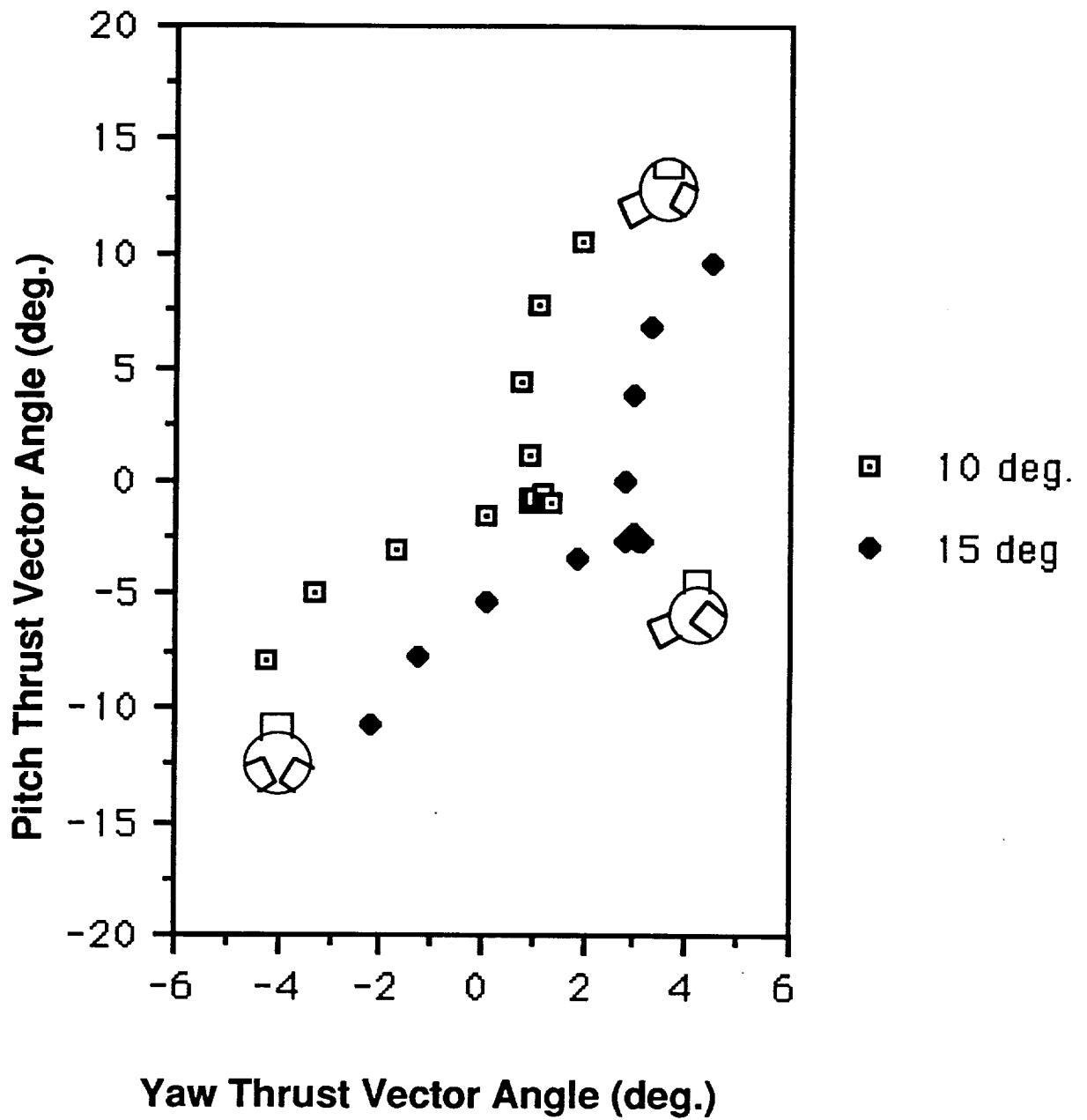
Figure 8. Resultant Thrust Vectoring Envelope for Maximum A/B-Power
Nozzle with One Vane Always Fully Retracted and Vane C Deployed at 10
and 15 degrees. NPR=3
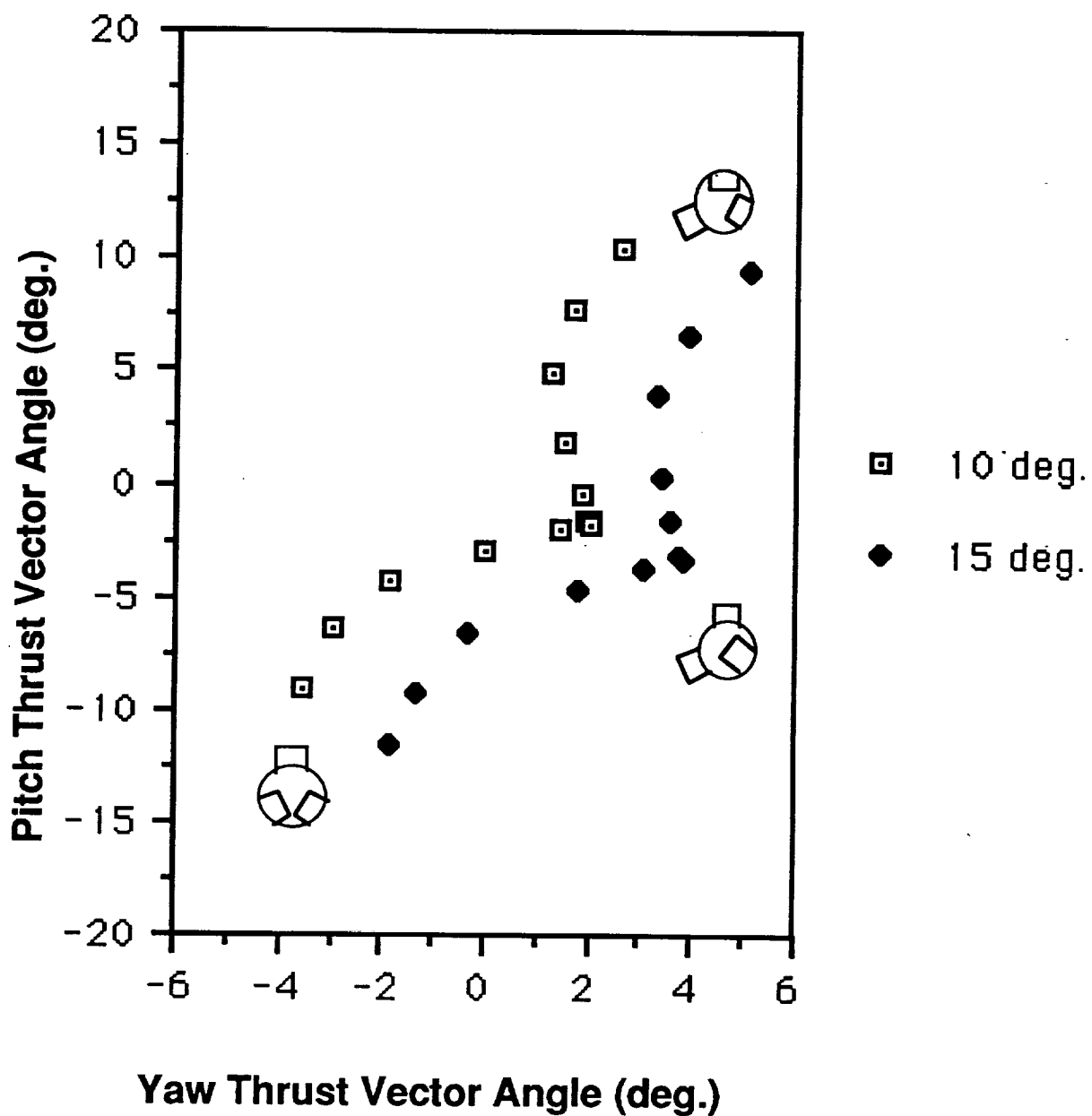
Figure 9. Resultant Thrust Vectoring Envelope for Maximum A/B-Power Nozzle with One Vane Always Retracted and Vane C Deployed at 10 and 15 Degrees. NPR=4
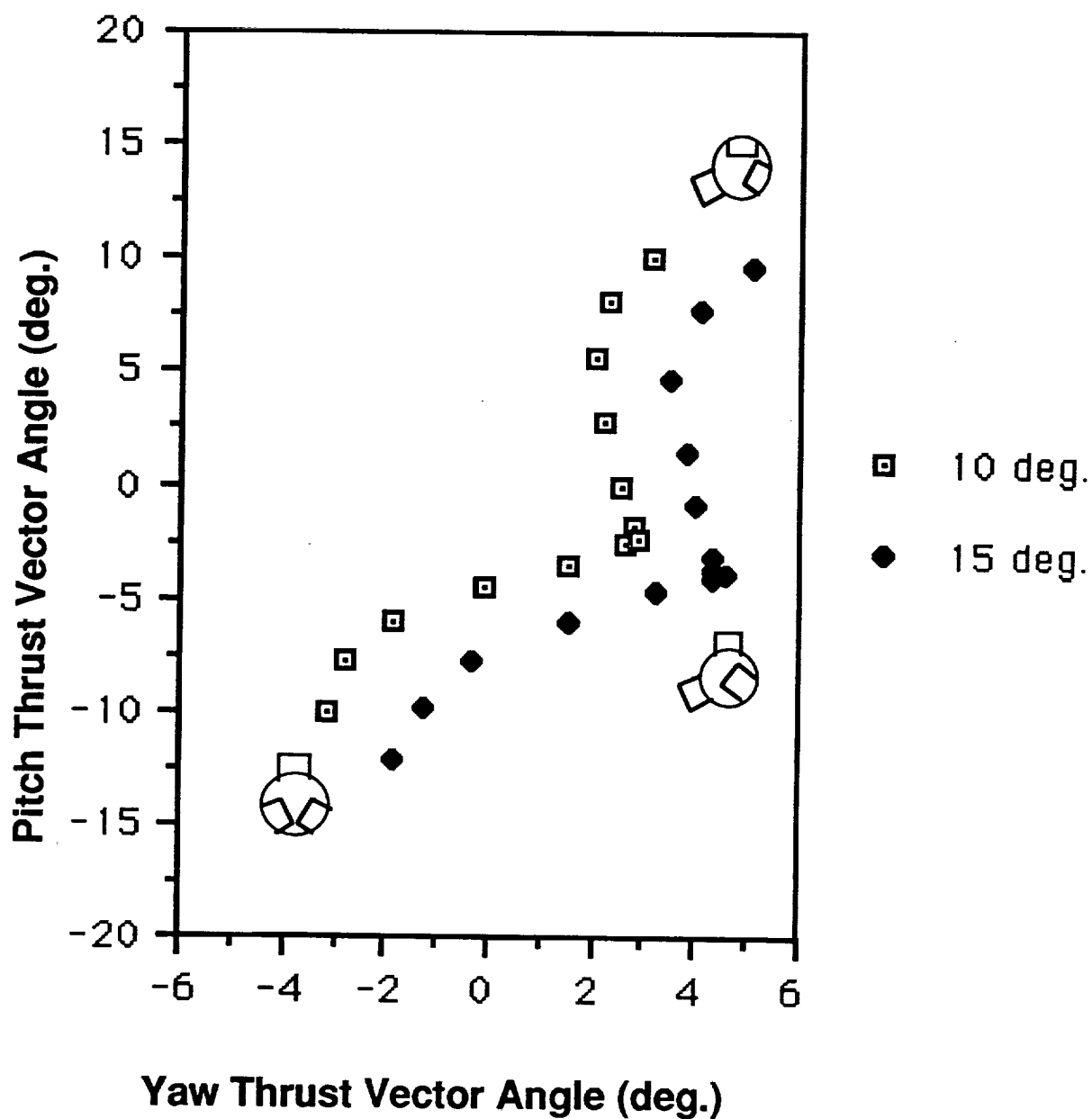
Figure 10. Resultant Thrust Vectoring Envelope for Maximum A/B-Power Nozzle with One Vane Always Retracted and Vane C Deployed at 10 and 15 Degrees. NPR=5
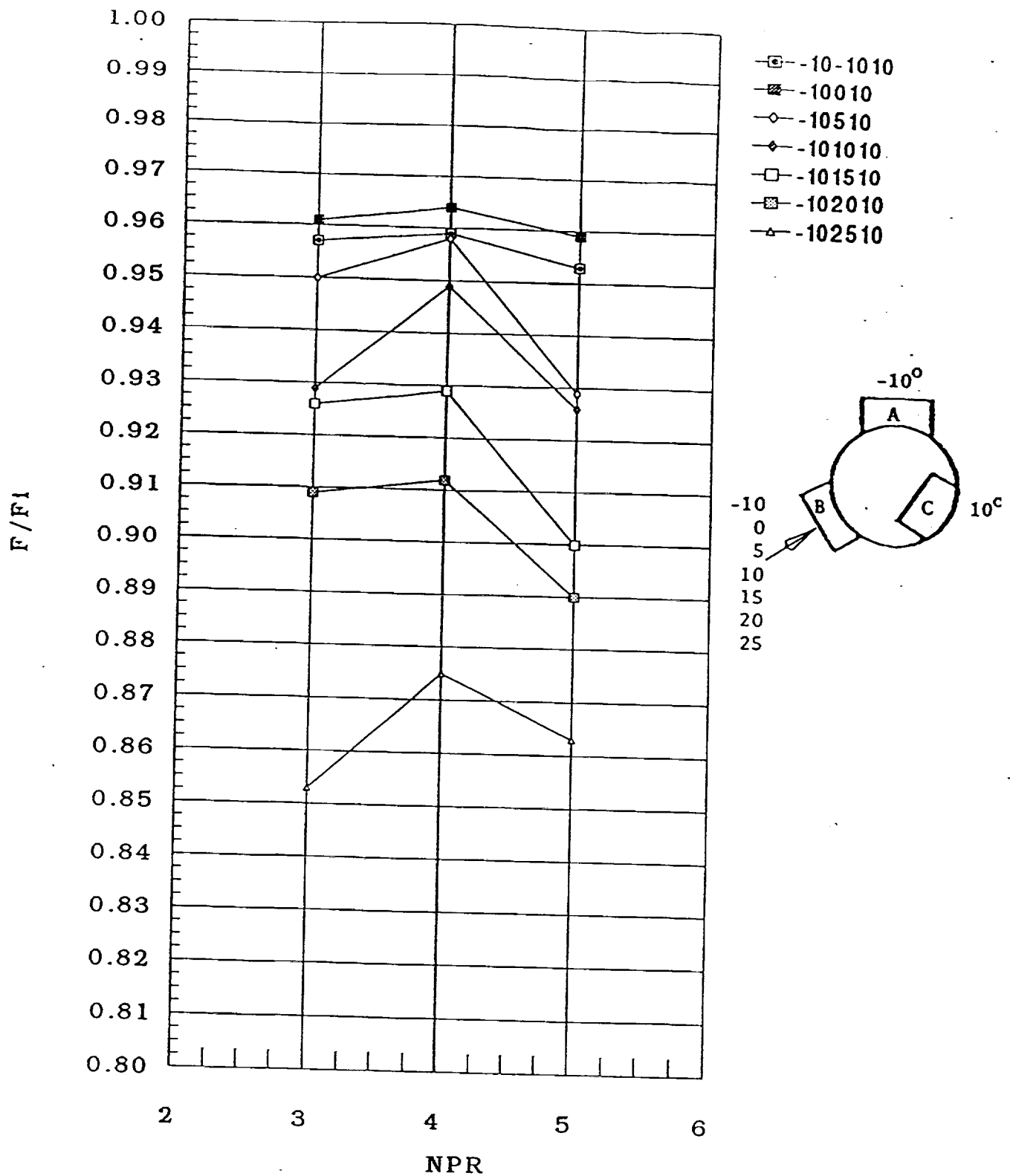
Appendix A
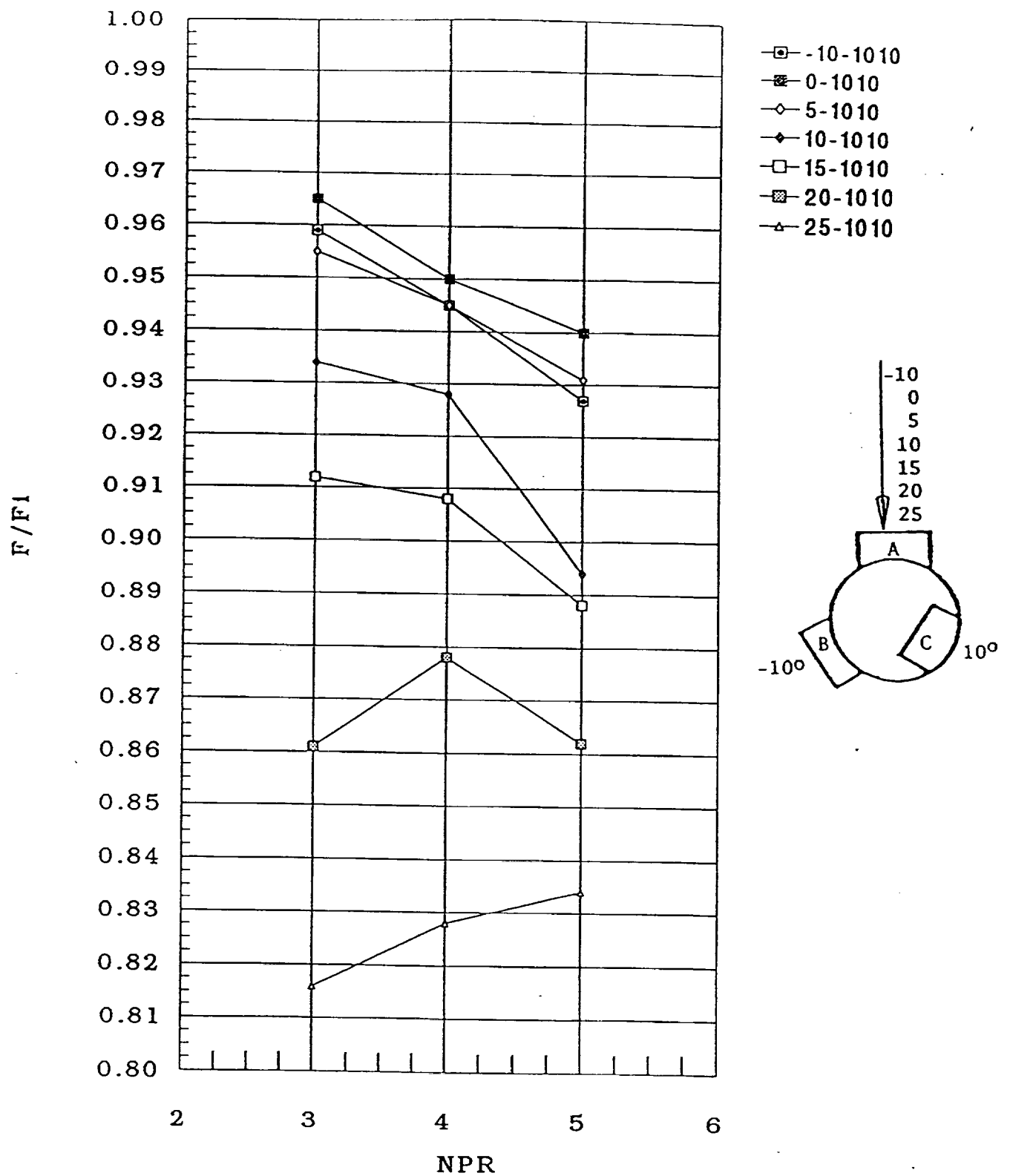
Figure 11a. Thrust Coefficient For Maximum A/B-Power Nozzle with
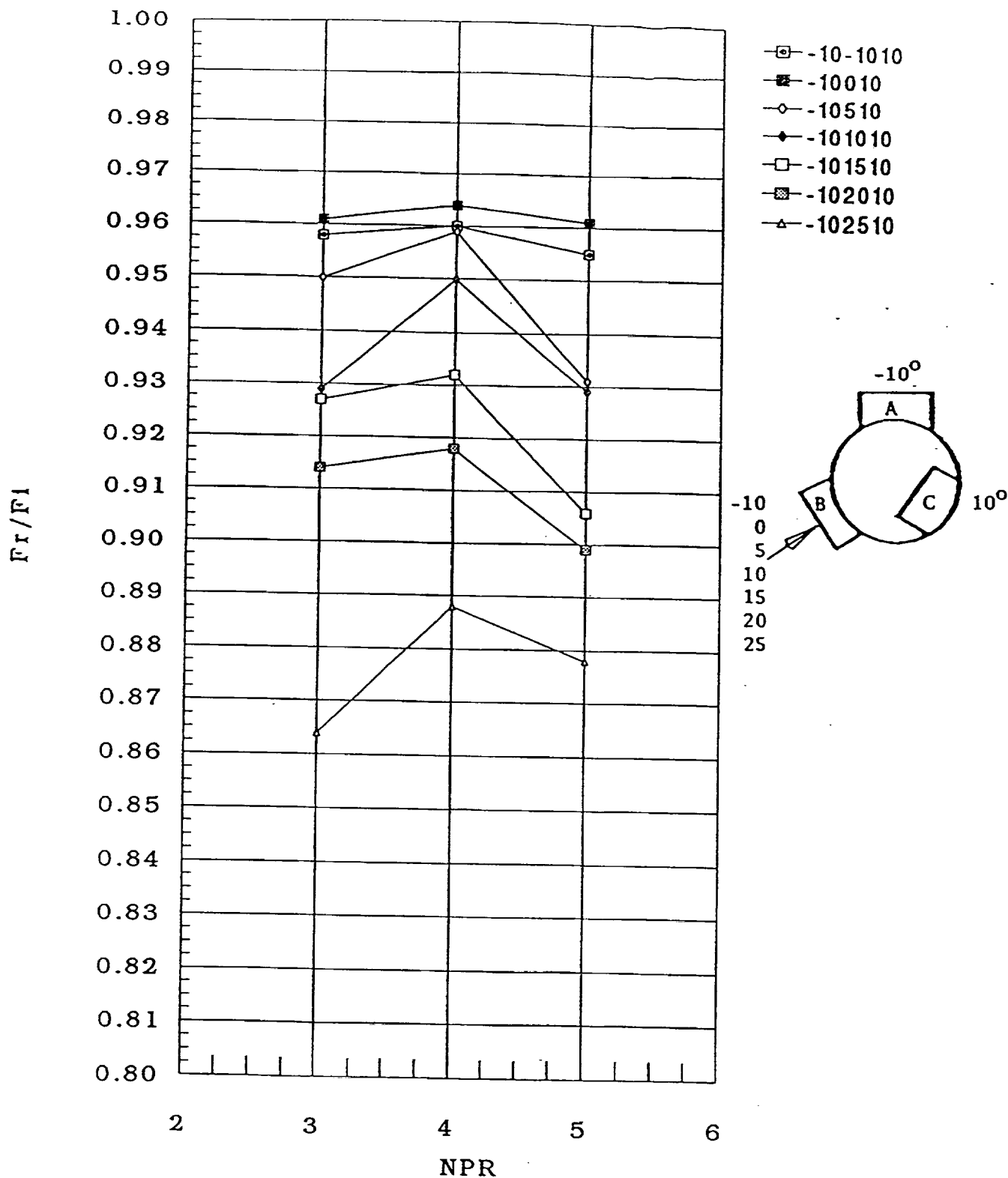Vanes A and C Deployed and Vane B Retracted
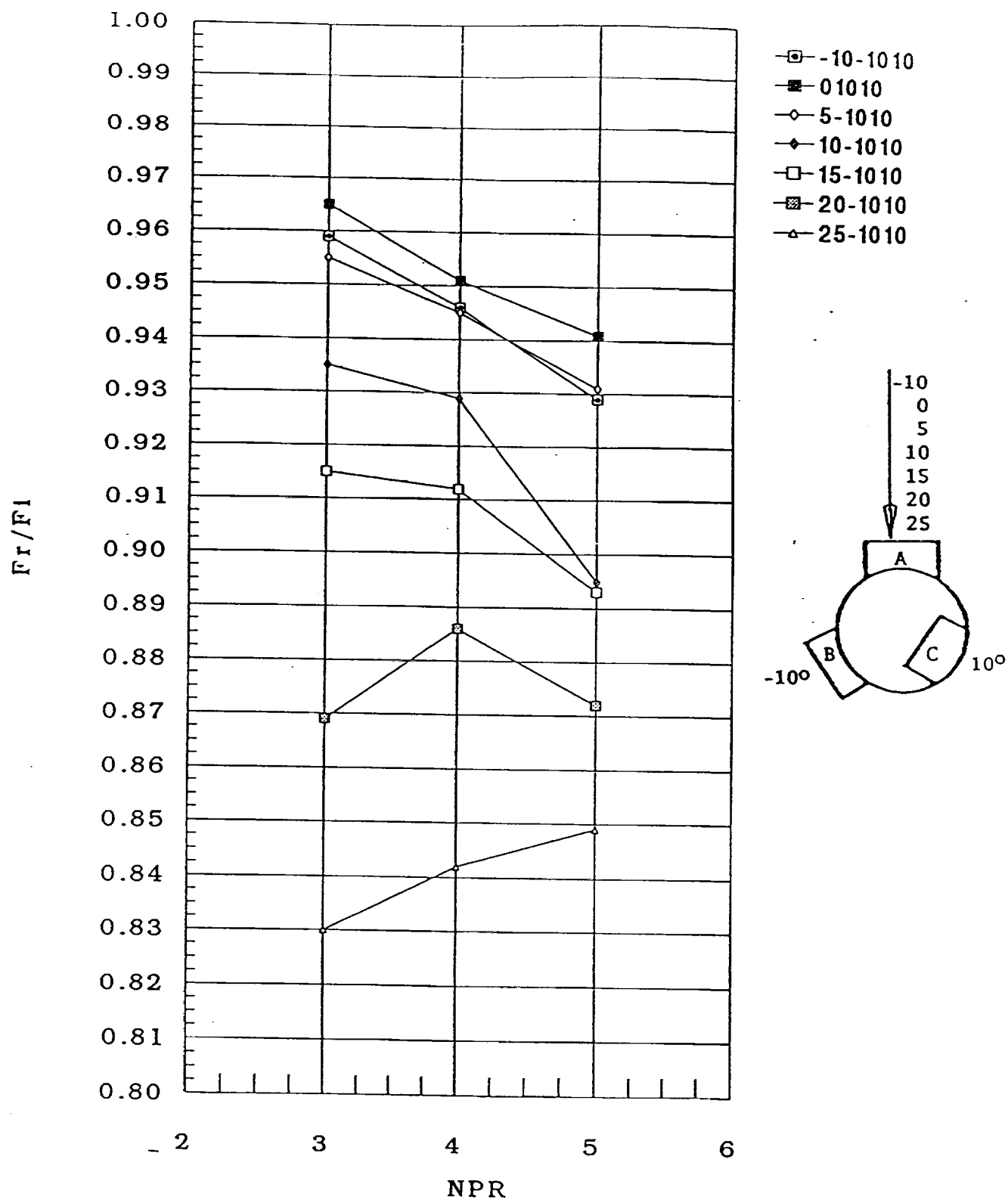
Figure 11b. Resultant Thrust Coefficient For Maximum A/B-Power Nozzle
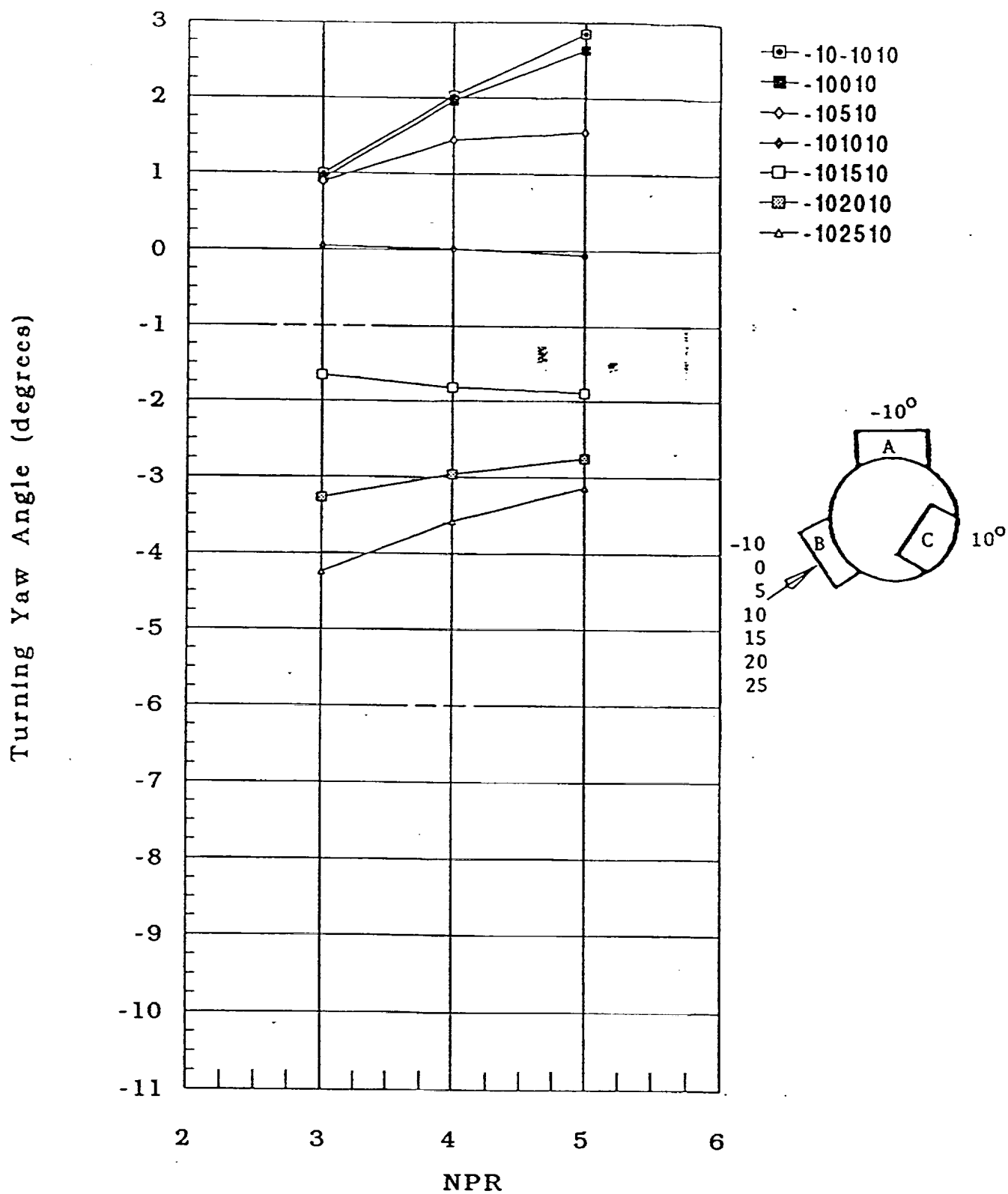with Vanes A and C Deployed and Vane B Fully Retracted
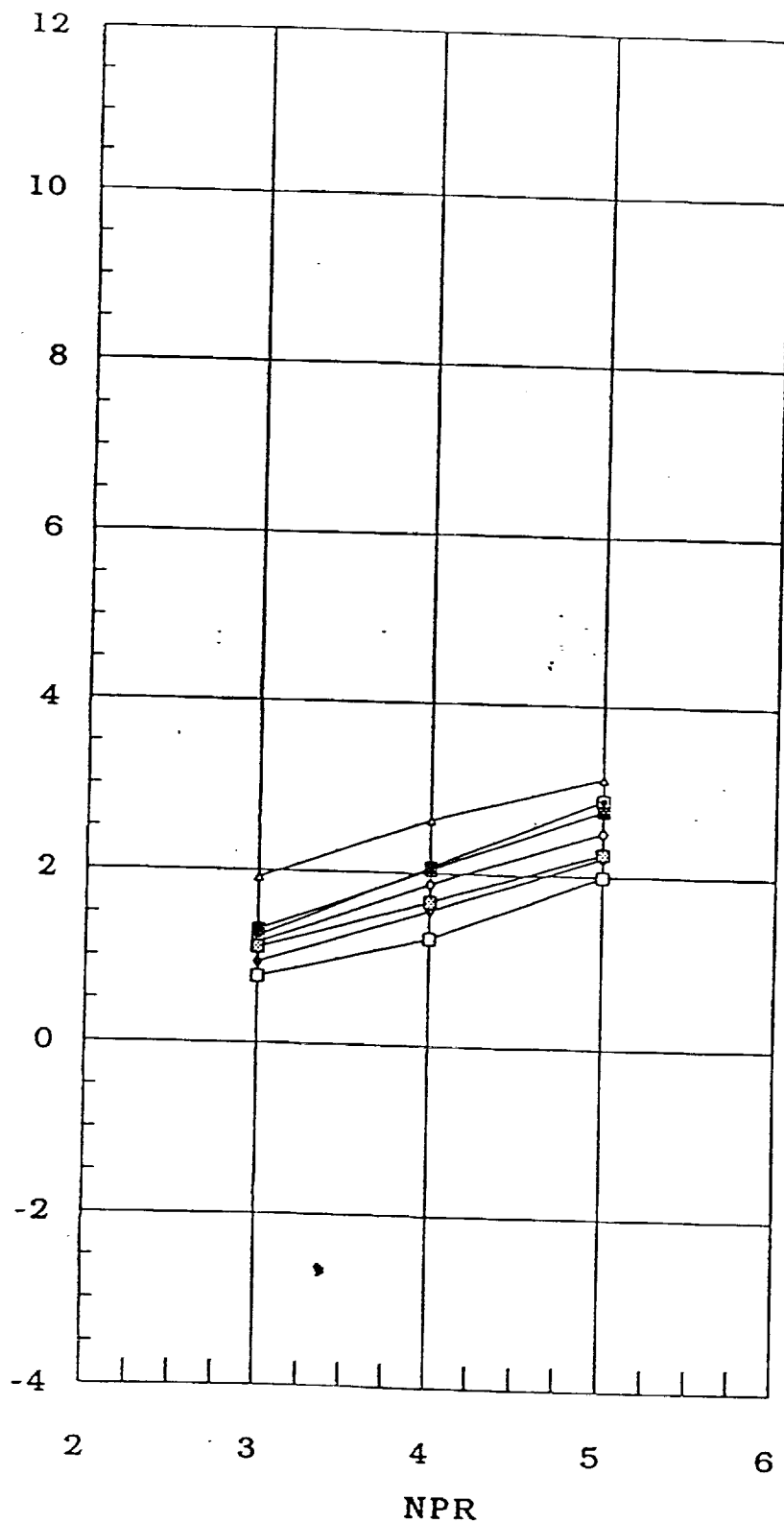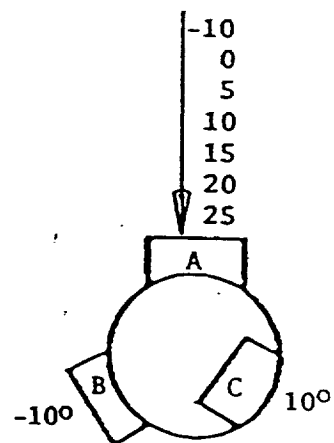
Figure 11c. Yaw Thrust Vector Performance For Maximum A/B-Power Nozzle with Vanes A and C Deployed and Vane B Retracted
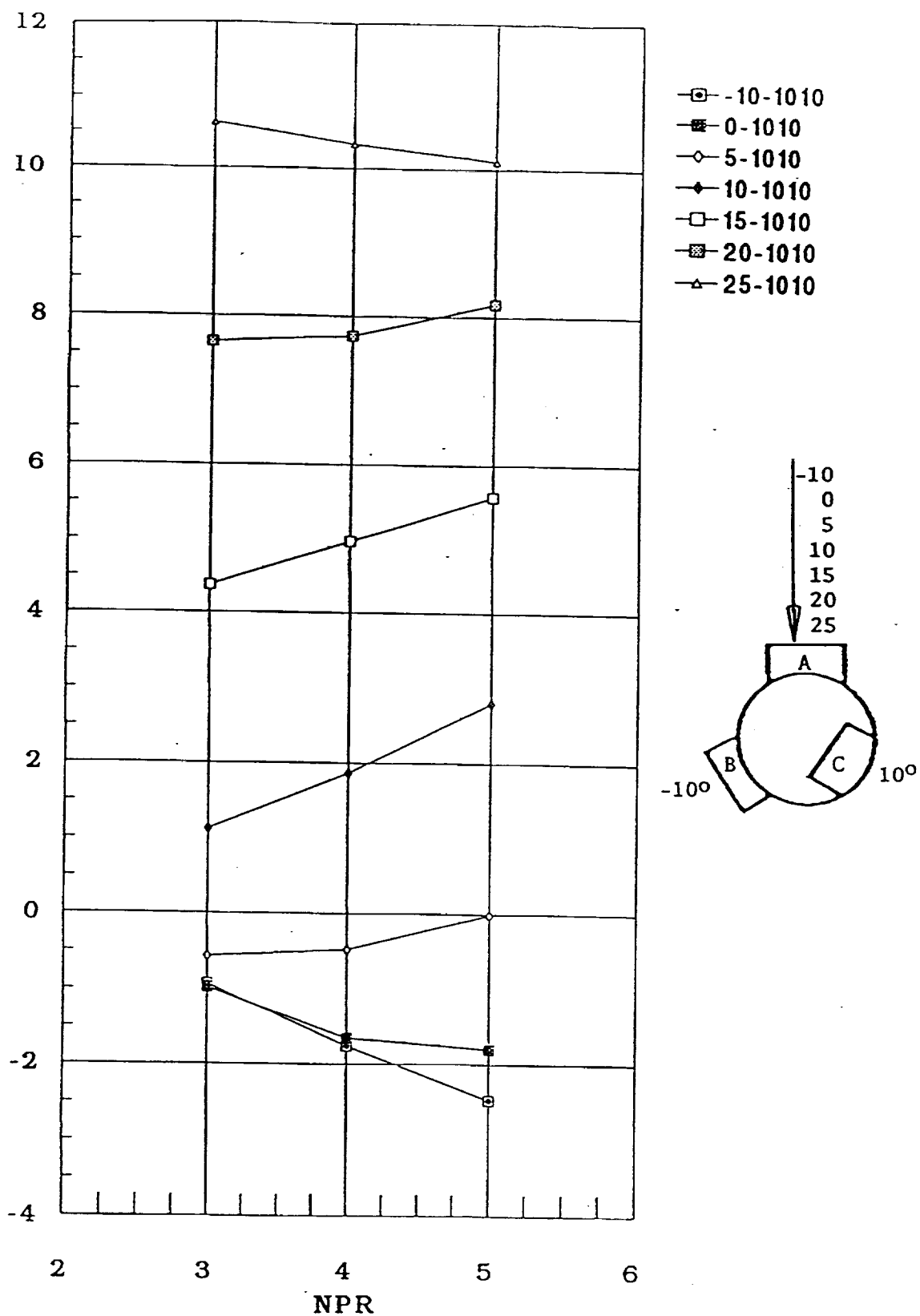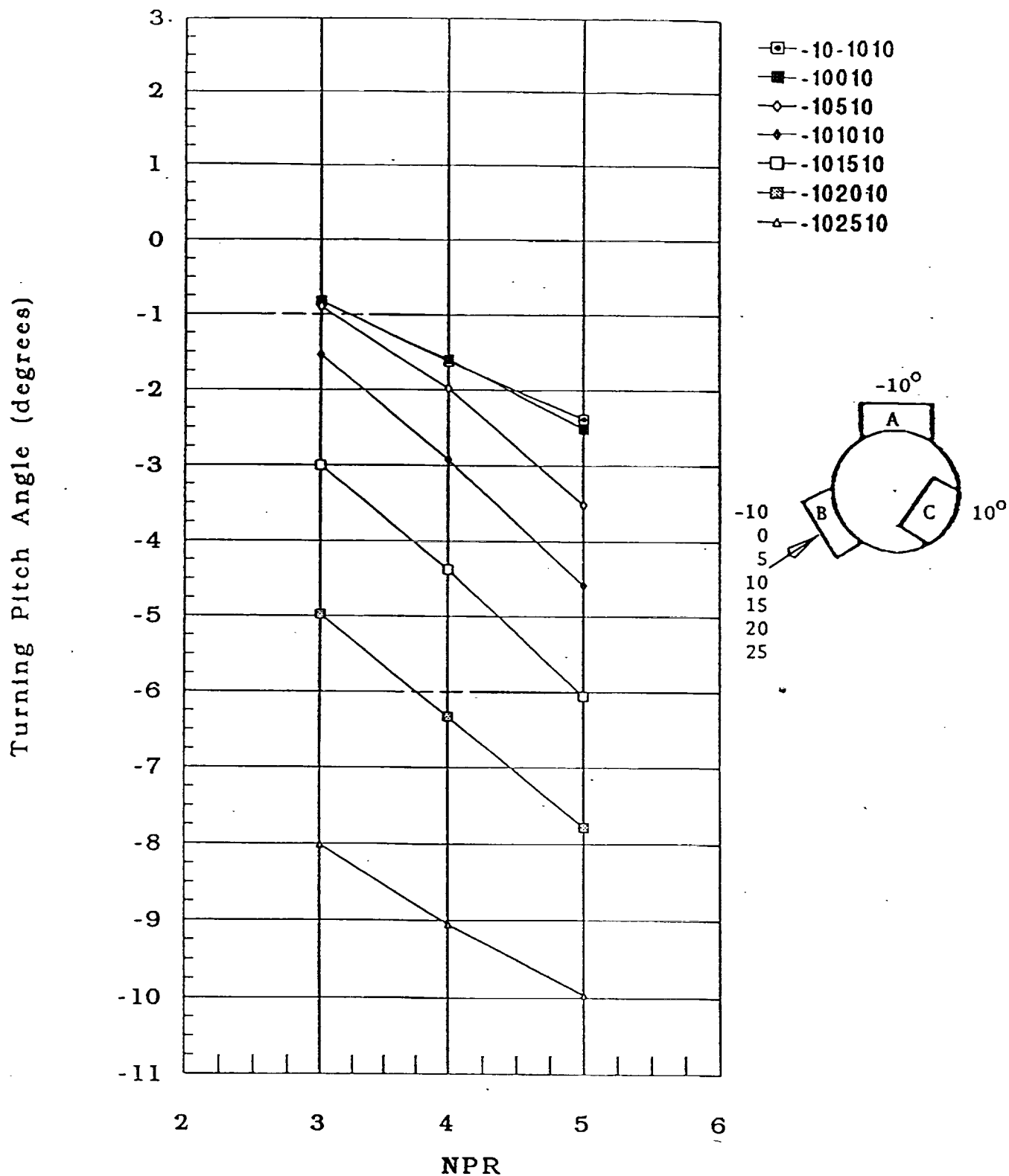
Figure 11d. Pitch Thrust Vector Performance For Maximum A/B-Power Nozzle
with Vanes A and C Deployed and Vane B Retracted

Figure 12a. Thrust Coefficient For Maximum A/B-Power Nozzle with
Vanes A and C Deployed and Vane B Retracted
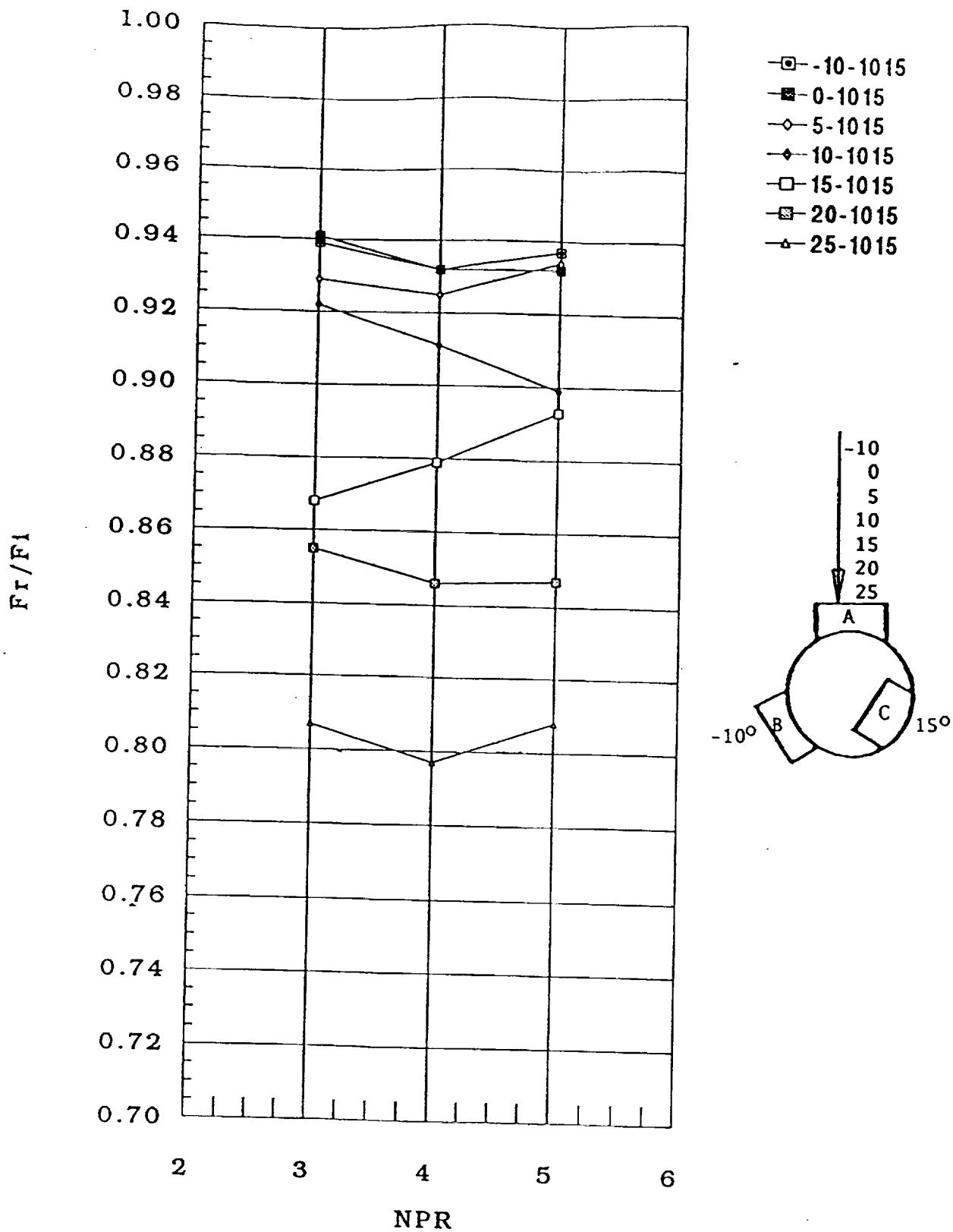
Figure 12b. Resultant Thrust Coefficient For Maximum A/B-Power Nozzle with Vanes A and C Deployed and Vane B Fully Retracted

Figure 12c. Yaw Thrust Vector Performance For Maximum A/B-Power Nozzle
with Vanes A and C Deployed and Vane B Retracted

40

Figure 12d. Pitch Thrust Vector Performance For Maximum A/B-Power Nozzle with Vanes A and C Deployed and Vane B Retracted
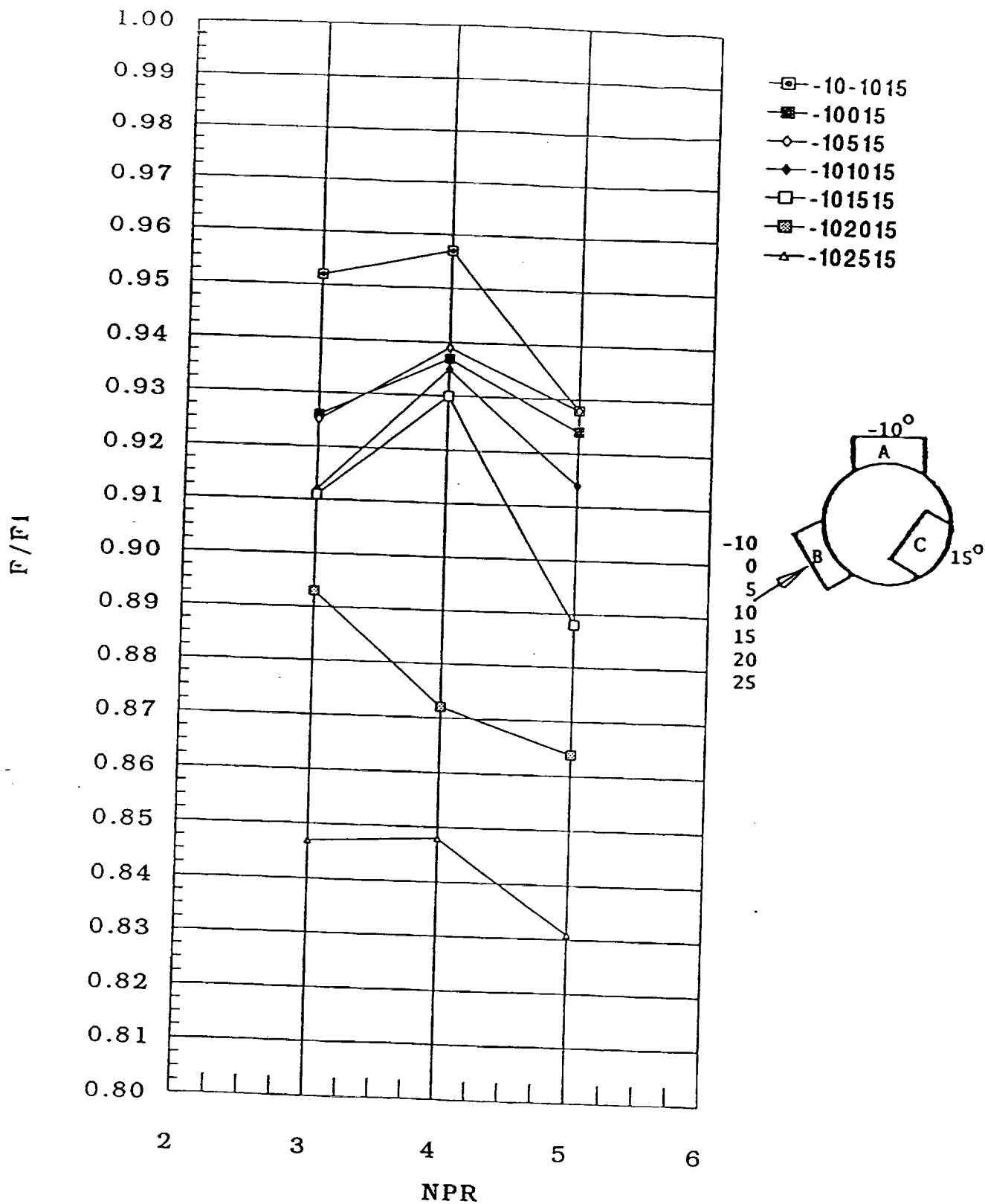
Figure 13a. Thrust Coefficient For Maximum A/B-Power Nozzle with
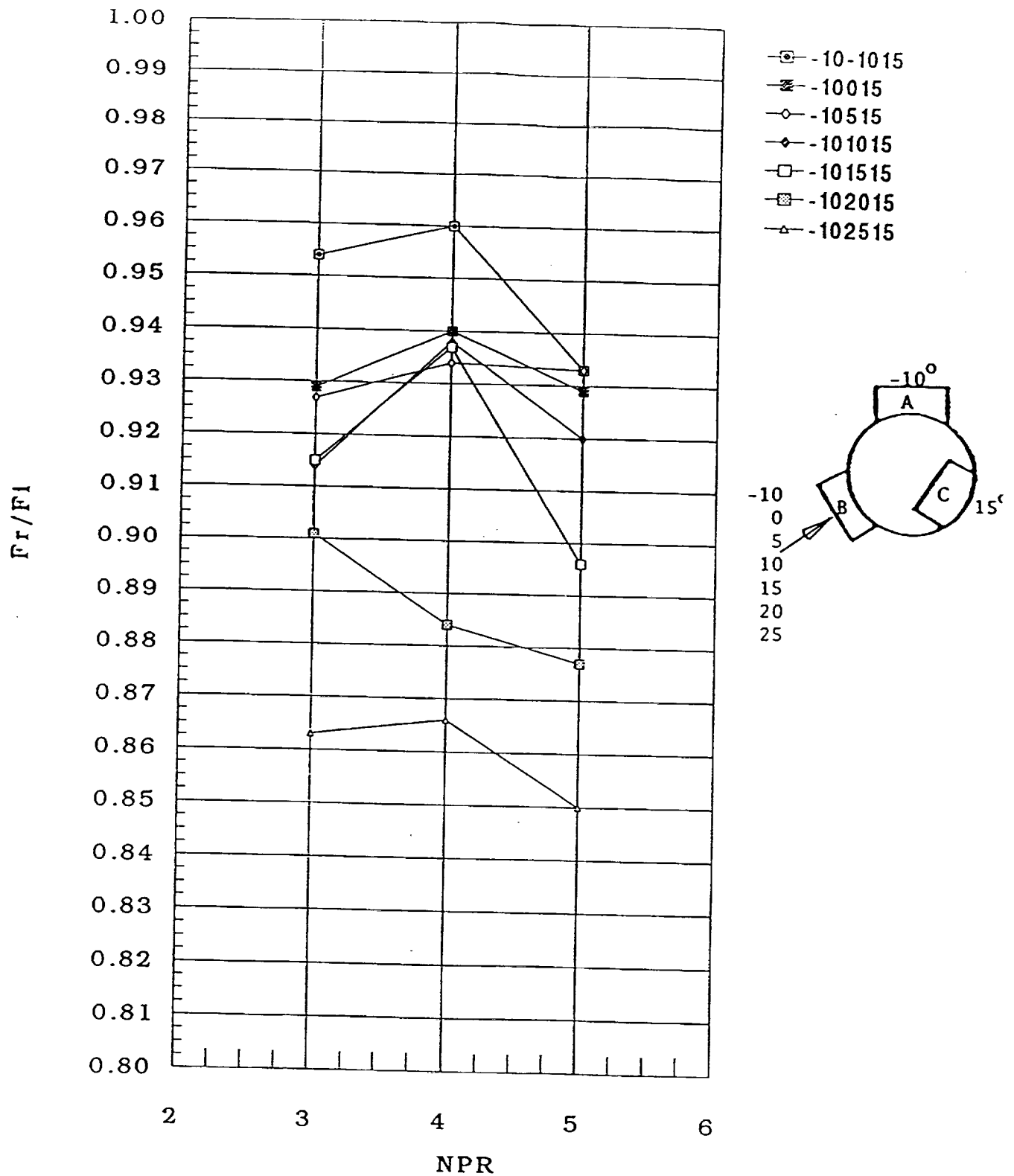Vanes B and C Deployed and Vane A Retracted

Figure 13b. Resultant Thrust Coefficient For Maximum A/B-Power Nozzle
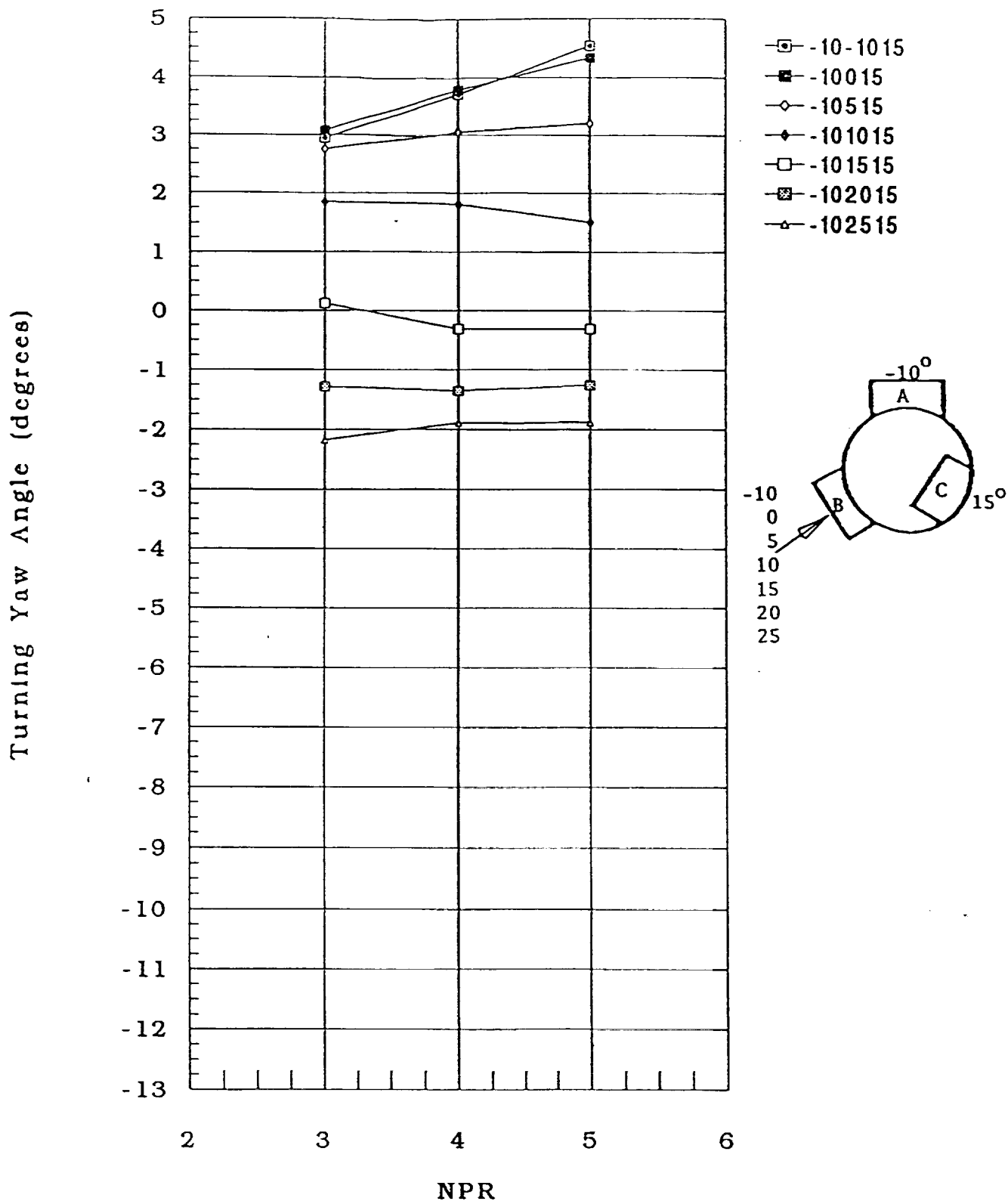with Vanes B and C Deployed and Vane A Fully Retracted

Figure 13c. Yaw Thrust Vector Performance For Maximum A/B-Power Nozzle
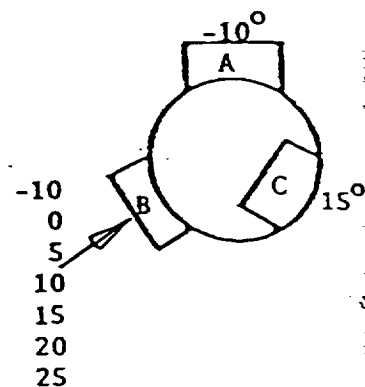with Vanes B and C Deployed and Vane A Retracted

Figure 13d. Pitch Thrust Vector Performance For Maximum A/B-Power Nozzle
with Vanes B and C Deployed and Vane A Retracted

45

Figure 14a. Thrust Coefficient For Maximum A/B-Power Nozzle with Vanes B and C Deployed and Vane A Retracted

Figure 14b. Resultant Thrust Coefficient For Maximum A/B-Power Nozzle
with Vanes B and C Deployed and Vane A Fully Retracted

Figure 14c. Yaw Thrust Vector Performance For Maximum A/B-Power Nozzle
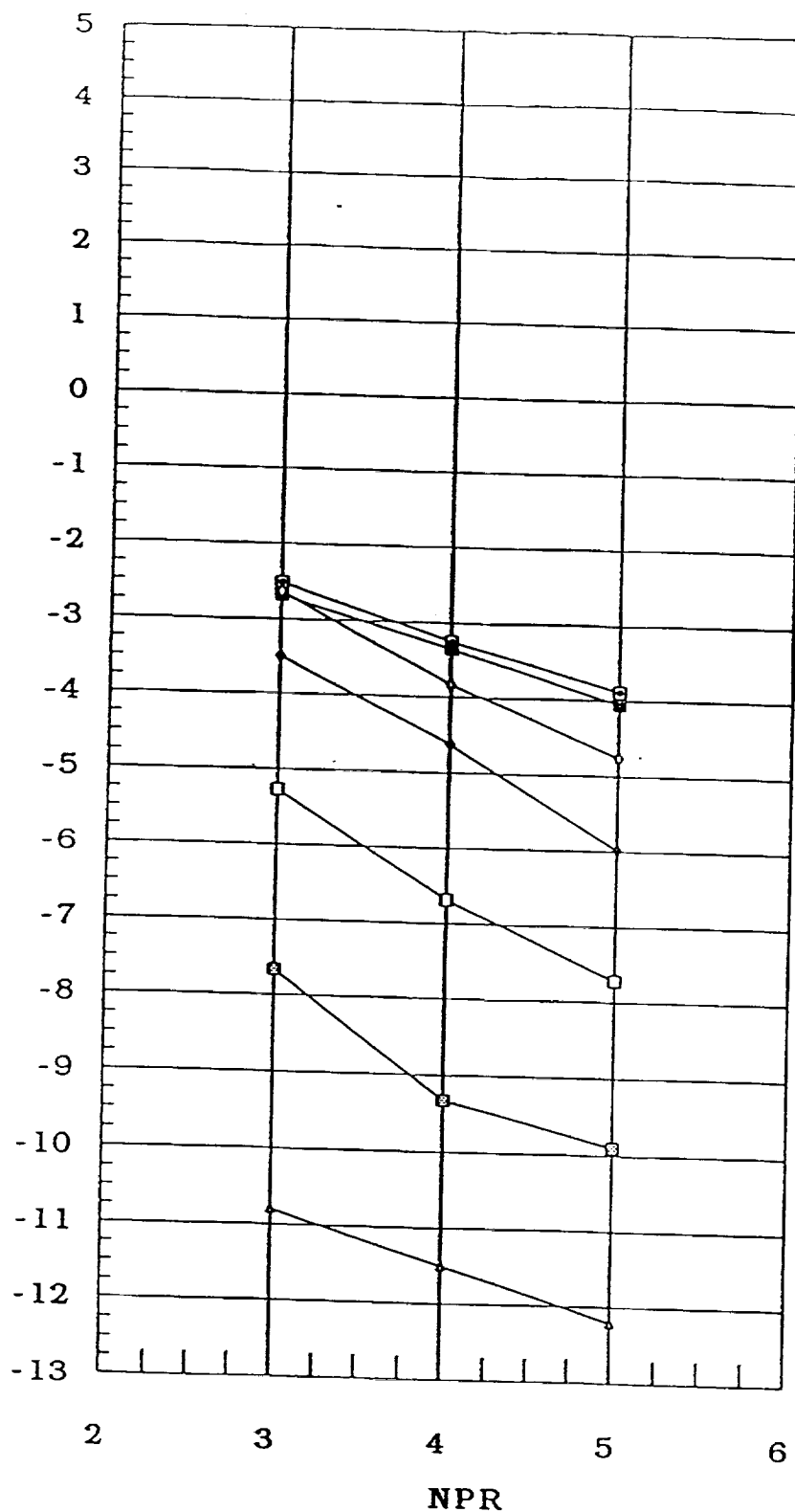with Vanes B and C Deployed and Vane A Retracted

Figure 14d. Pitch Thrust Vector Performance For Maximum A/B-Power Nozzle
with Vanes B and C Deployed and Vane A Retracted